

## Article

# A Modified Blasingame Production Analysis Method for Vertical Wells Considering the Quadratic Gradient Term

Junjie Ren \*, Qiao Zheng and Chunlan Zhao

School of Sciences, Southwest Petroleum University, Chengdu 610500, Sichuan, China;  
zhengqiaotzq@126.com (Q.Z.); your\_wang1119@sina.com (C.Z.)

\* Correspondence: renjunjie1900@126.com; Tel.: +86-028-8303-7669

Received: 22 March 2019; Accepted: 29 May 2019; Published: 31 May 2019



**Abstract:** Fluid flow in actual oil reservoirs is consistent with material balance, which should be described by the nonlinear governing equation, including the quadratic gradient term (QGT). Nonetheless, the widely-used Blasingame production decline analysis (BPDA) is established based on the conventional governing equation neglecting the QGT, which leads to some errors in the interpretation of production data under some conditions, such as wells producing at a large drawdown pressure. This work extends BPDA to incorporate the effect of the QGT by modifying material balance time and normalized rate functions. The step-by-step procedure for the proposed production decline analysis (PPDA) is presented and compared with that for BPDA. The simulated cases for various production scenarios are used to validate PPDA. A field case is employed to show the applicability of PPDA in practice. Comparisons between the results obtained by BPDA and PPDA are analyzed in detail. It is found that BPDA overestimates the permeability and original oil-in-place, while PPDA works well. Compared with BPDA, PPDA can be employed to obtain more accurate original oil-in-place and reservoir properties, especially when wells produce at a large drawdown pressure.

**Keywords:** production decline analysis; oil reservoir; material balance; quadratic gradient term; Blasingame type curve

## 1. Introduction

Production decline analysis is considered to be an important reservoir engineering method for reservoir characterization and evaluation in the development of oil reservoirs, where production data is employed to estimate reservoir properties (e.g., formation permeability) and original oil-in-place [1–4]. Over the last decades, pressure response analysis and production decline analysis have received much attention owing to their low cost and high reliability [5–15].

The first production decline analysis was published in 1945, when Arps [16] proposed the empirical decline relations including exponential relation, hyperbolic relation, and harmonic relation. The original version of Arps' production decline analysis is only applicable to the cases of wells producing at a constant bottomhole pressure during the boundary dominated flow period, and then the modified versions were proposed to deal with various production conditions in different reservoir scenarios [17,18]. However, as an empirical tool, Arps production decline analysis is usually used to estimate recoverable reserve and cannot be employed to obtain reservoir properties. With the assumption of wells producing at a constant bottomhole pressure, Fetkovich and his co-workers provided a theoretical basis for Arps' method and proposed a new methodology for production decline analysis [19–21]. Although Fetkovich production decline analysis can be employed to estimate reservoir properties and original oil-in-place, it is limited in the cases of a well producing at a constant

bottomhole pressure. In order to deal with the variable-rate/pressure cases, Blasingame et al. [22] proposed a function of time (i.e., material balance time) that can transform a variable-rate/pressure system into an equivalent constant-rate system. Then Blasingame and his co-workers developed production decline analysis for variable-rate/pressure cases based on material balance time, which was known as BPDA [23,24]. From then on, BPDA received extensive attention and was extended to different well types and reservoir scenarios. Doublet and Blasingame [25] developed BPDA for an infinite-conductivity fractured vertical well, which can be employed to estimate fracture half-length. Marhaendrajana and Blasingame [26] proposed an analytical solution for a multiwall reservoir system and developed BPDA for a multiwall reservoir system. Pratikno et al. [27] improved Blasingame type curves and proposed BPDA for a finite-conductivity fractured vertical well. Nie et al. [28] investigated Blasingame type curves of a horizontal well in a naturally fractured reservoir based on an analytical model. Wang et al. [29] established Blasingame type curves of multiple fractured horizontal wells (MFHWs) and made a sensitivity analysis of type curves. Although BPDA has been developed to interpret production data of various wells in different reservoir scenarios, BPDA is established based on the conventional governing equation without the quadratic gradient term (QGT), which is inconsistent with material balance. The governing equation, describing fluid flow through porous media, is a nonlinear partial differential equation because of the presence of the QGT. This nonlinear equation is usually linearized by neglecting the QGT with the assumption of small pressure gradients. However, the linearized equation with neglecting the QGT may cause significant errors in the prediction of the transient pressure/flow rate during certain operations such as large-pressure-gradient production. Over the last decades, transient pressure/flow rates considering the impact of the QGT has received much attention. Many scholars established seepage models with the QGT and studied the effect of the QGT on pressure behaviors for various wells under a constant-rate-production (CRP) condition, including vertical wells [30–32], horizontal wells [33], and MFHWs [34,35]. It was found that due to neglecting the QGT, there may be a large error in predicting transient pressure, when wells produce at a large flow rate or for a long time. Recently, Ren and Guo [36] made a detailed analysis of the relationship between the seepage models with and without the QGT, and investigated the characteristics of a transient flow rate under a constant-pressure-production (CPP) condition. It was found that if the effect of the QGT is neglected, transient flow rate is underestimated. Fluid flow in actual reservoirs is consistent with material balance, which should be described by the nonlinear governing equation with the QGT; thus, BPDA based on the conventional governing equation without the QGT may lead to some errors in the interpretation of production data under some conditions.

In this work, we extended BPDA to incorporate the impact of the QGT by modifying material balance time and normalized rate functions, and then simulated cases for various production scenarios were used to validate PPDA. Finally, comparisons between BPDA and PPDA were discussed in detail.

## 2. Theory and Analysis

In this section, we discuss the theory for production decline analysis based on the governing equation with the QGT in detail. A completely penetrating vertical well was considered here, while the derived theory and developed method for production decline analysis are easily extended to various well types. The schematic of the physical model for a vertical well in a finite closed reservoir is shown in Figure 1, and the assumptions are given as follows:

- (1) A completely penetrating vertical well is located at the center of a finite closed reservoir with a constant thickness. Single-phase liquid can be exploited by the vertical well with variable rates and bottomhole pressures.
- (2) A homogeneous and isotropic reservoir with constant permeability and porosity is considered. The compressibility of the slightly compressible rock keeps constant.
- (3) The compressibility and viscosity of the fluid are considered to be constant. Fluid flow in the reservoir is consistent with the Darcy law.
- (4) The initial pressure is uniformly distributed in the reservoir.

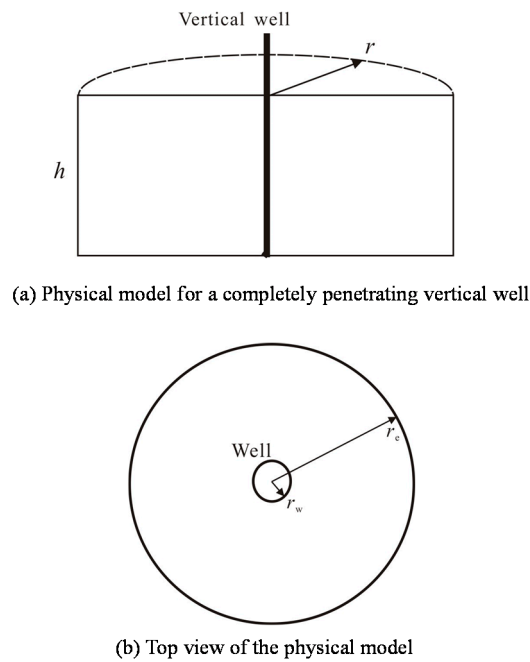


**Figure 1.** Schematic of the physical model for a vertical well in a finite closed reservoir.

### 2.1. Governing Equations

The continuity equation in a radial coordinate system is [37,38]:

$$\frac{1}{r} \frac{\partial(rpv)}{\partial r} = \frac{\partial(\rho\phi)}{\partial t}. \quad (1)$$

The Darcy law is expressed as:

$$v = \frac{k}{\mu} \frac{\partial p}{\partial r}. \quad (2)$$

The fluid compressibility is introduced as follows:

$$c_f = \frac{1}{\rho} \frac{\partial \rho}{\partial p}. \quad (3)$$

The rock compressibility is defined as follows:

$$c_r = \frac{1}{\phi} \frac{\partial \phi}{\partial p}. \quad (4)$$

With the aid of Equations (1)–(4), the governing equation with the QGT is derived as (Appendix A):

$$\frac{1}{r} \frac{\partial}{\partial r} \left( r \frac{\partial p}{\partial r} \right) + c_t \left( \frac{\partial p}{\partial t} \right)^2 = \frac{\phi \mu c_t}{k} \frac{\partial p}{\partial t}, \quad (5)$$

where  $c_t$  is the total compressibility expressed by  $c_t = c_f + c_r$ .

If the second term of Equation (5) is neglected, Equation (5) is reduced to the conventional governing equation without the QGT [39]:

$$\frac{1}{r} \frac{\partial}{\partial r} \left( r \frac{\partial p}{\partial r} \right) = \frac{\phi \mu c_t}{k} \frac{\partial p}{\partial t}. \quad (6)$$

## 2.2. Relationship between the Seepage Models of Vertical Wells with and without the Effect of the QGT

Recently, we conducted a detailed analysis of the relationship between seepage models with and without the effect of the QGT [36]. We briefly reviewed this as follows:

The seepage model of vertical wells in finite closed reservoirs based on the governing equation with the QGT can be linearized as [36]:

$$\frac{1}{r} \frac{\partial}{\partial r} \left( r \frac{\partial \Delta p^*}{\partial r} \right) = \frac{\phi \mu c_t}{k} \frac{\partial \Delta p^*}{\partial t}, \quad (7)$$

$$\Delta p^*|_{t=0} = 0, \quad (8)$$

$$\frac{\partial \Delta p^*}{\partial r} \Big|_{r=r_e} = 0, \quad (9)$$

$$q^*(t) = -\frac{2\pi kh}{\mu B} \left( r \frac{\partial \Delta p^*}{\partial r} \right) \Big|_{r=r_w}, \quad (10)$$

where

$$\Delta p^* = \exp(-c_f \Delta p) - 1, \quad (11)$$

$$q^*(t) = -q(t)c_f \exp(-c_f \Delta p), \quad (12)$$

where  $\Delta p = p_i - p$ . It is obvious that the seepage model with respect to  $\Delta p^*$  and  $q^*$  considering the effect of the QGT is equivalent to the seepage model with respect to  $\Delta p$  and  $q$  neglecting the effect of the QGT.

## 2.3. Brief Review of the Theory for BPDA

In order to interpret the variable-rate/pressure data, Blasingame et al. [22] introduced the concepts of material balance time and normalized rate function, and then bridged the gap between the CPP and CRP conditions.

### 2.3.1. Dimensionless Seepage Model under the CPP Condition

The Laplace-space dimensionless pressure solution of the seepage model of vertical wells in finite closed reservoirs under the CPP condition can be obtained by (Appendix B):

$$\bar{p}_D = \frac{K_1(r_{eD} \sqrt{s}) I_0(\sqrt{s} r_{D}) + I_1(r_{eD} \sqrt{s}) K_0(\sqrt{s} r_{D})}{s [I_0(\sqrt{s}) K_1(r_{eD} \sqrt{s}) + K_0(\sqrt{s}) I_1(r_{eD} \sqrt{s})]}, \quad (13)$$

where the definitions of dimensionless variables for CPP cases are listed in Table 1.

The dimensionless flow rate  $q_D$  for vertical wells under the CPP condition is expressed as:

$$q_D = -\frac{\partial p_D}{\partial r_D} \Big|_{r_D=1}. \quad (14)$$

With the aid of Equations (13) and (14), we can obtain the dimensionless flow rate in Laplace space as follows:

$$\bar{q}_D = \frac{I_1(r_{eD} \sqrt{s}) K_1(\sqrt{s}) - K_1(r_{eD} \sqrt{s}) I_1(\sqrt{s})}{\sqrt{s} [I_0(\sqrt{s}) K_1(r_{eD} \sqrt{s}) + K_0(\sqrt{s}) I_1(r_{eD} \sqrt{s})]}. \quad (15)$$

**Table 1.** Definitions of dimensionless variables for vertical wells.

Nomenclature	CPP Case	CRP Case
Dimensionless pressure	$p_D = \frac{p_i - p}{p_i - p_w} = \frac{\Delta p}{\Delta p_w}$	$p_D = \frac{2\pi kh \Delta p}{q B \mu}$
Dimensionless bottomhole pressure	$p_{wD} = 1$	$p_{wD} = \frac{2\pi kh \Delta p_w}{q B \mu}$
Dimensionless time	$t_D = \frac{kt}{\phi c_t \mu r_w^2}$	$t_D = \frac{kt}{\phi c_t \mu r_w^2}$
Dimensionless distance	$r_D = \frac{r}{r_w}, r_{eD} = \frac{r_e}{r_w}$	$r_D = \frac{r}{r_w}, r_{eD} = \frac{r_e}{r_w}$
Dimensionless flow rate	$q_D = \frac{q B \mu}{2\pi kh \Delta p_w}$	$q_D = 1$

### 2.3.2. Dimensionless Seepage Model under the CRP Condition

The Laplace-space dimensionless bottomhole pressure of vertical wells in finite closed reservoirs under the CRP condition is derived as follows (Appendix C):

$$\bar{p}_{wD} = \bar{p}_D|_{r_D=1} = \frac{K_1(r_{eD} \sqrt{s}) I_0(\sqrt{s}) + I_1(r_{eD} \sqrt{s}) K_0(\sqrt{s})}{s \sqrt{s} [K_1(\sqrt{s}) I_1(r_{eD} \sqrt{s}) - I_1(\sqrt{s}) K_1(r_{eD} \sqrt{s})]}, \quad (16)$$

where the definitions of dimensionless variables for CRP cases are listed in Table 1.

With the aid of the Stehfest inversion method [40],  $q_D(t_D)$  under the CPP condition and  $p_{wD}(t_D)$  under the CRP condition can be obtained based on Equations (15) and (16), respectively.

### 2.3.3. Material Balance Time and Normalized Rate Function

In order to establish the relationship between  $q_D(t_D)$  under the CPP condition and  $p_{wD}(t_D)$  under the CRP condition, dimensionless material balance time was introduced as [22]:

$$t_{cD} = \frac{1}{q_D} \int_0^{t_D} q_D(\tau) d\tau, \quad (17)$$

where  $t_{cD}$  is the dimensionless material balance time defined by  $t_{cD} = kt_c / (\phi c_t \mu r_w^2)$ ;  $t_c$  is the material balance time expressed by  $t_c = \int_0^t q(\tau) d\tau / q$ . It is obvious that  $t_{cD}$  is equal to  $t_D$  under the CRP condition.

It was found that the “ $q_D$  vs.  $t_{cD}$ ” curve for the CPP case almost coincided with the “ $1/p_{wD}$  vs.  $t_{cD}$ ” curve (i.e., the “ $1/p_{wD}$  vs.  $t_D$ ” curve) for the CRP case, which is shown in Figure 2. According to the definitions of  $q_D$  in the CPP case and  $p_{wD}$  in the CRP case shown in Table 1, it is obvious from Figure 2 that the curves of  $q/\Delta p_w$  versus  $t_c$  for both the CPP and CRP cases are almost the same. Therefore, normalized rate function ( $q/\Delta p_w$ ) and material balance time ( $t_c$ ) can be employed to transform a variable-rate/pressure system into a constant-rate system [22].

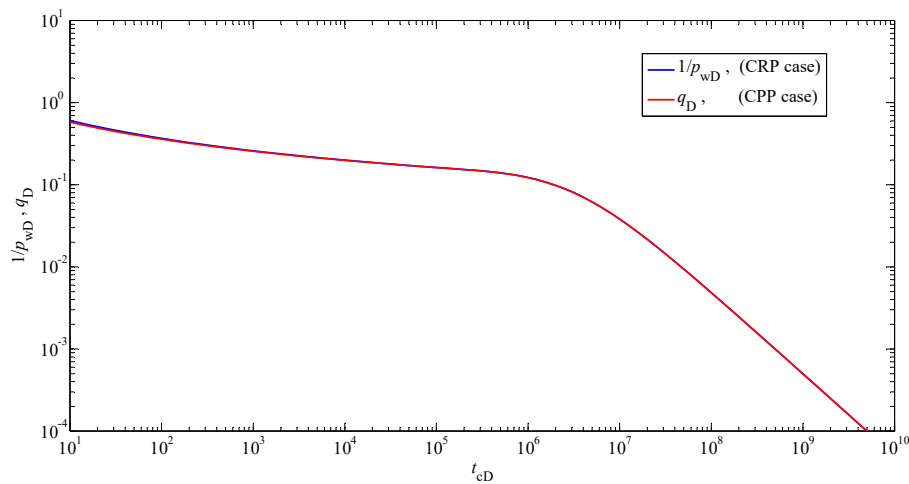


**Figure 2.** Comparison between the “ $1/p_{wD}$  vs.  $t_{cD}$ ” curve for the CRP case and the “ $q_D$  vs.  $t_{cD}$ ” curve for the CPP case.

#### 2.4. Modified Material Balance Time and Modified Normalized Rate Function

Although BPDA has been widely used to interpret production data and obtain reservoir properties and original oil-in-place, it is established on the basis of the conventional governing equation without the QGT. Because the conventional governing equation is inconsistent with material balance, BPDA may lead to some errors in interpreting production data. Considering the relationship between the seepage models with and without the effect of the QGT, we modified material balance time and normalized rate function, and then developed BPDA.

The seepage model with the QGT related to  $\Delta p^*$  and  $q^*$  is equivalent to that without the QGT related to  $\Delta p$  and  $q$ . Following the derivation of BPDA presented above, we proposed the theory for modified BPDA.

Similar to the definitions of dimensionless variables with respect to  $\Delta p$  and  $q$  shown in Table 1, the definitions of pseudo-dimensionless and dimensionless variables with respect to  $\Delta p^*$  and  $q^*$  are listed in Table 2. In the same way, if oil wells produce at a constant transformed pressure difference  $\Delta p_w^* = \exp(-c_f \Delta p_w) - 1$ , the seepage model of vertical wells in finite closed reservoirs based on the governing equation with the QGT is given by:

$$\frac{1}{r_D} \frac{\partial}{\partial r_D} \left( r_D \frac{\partial p_D^*}{\partial r_D} \right) = \frac{\partial p_D^*}{\partial t_D}, \quad (18)$$

$$p_D^*|_{t_D=0} = 0, \quad (19)$$

$$\frac{\partial p_D^*}{\partial r_D} \bigg|_{r_D=r_{eD}} = 0, \quad (20)$$

$$p_D^*|_{r_D=1} = 1, \quad (21)$$

where  $p_D^*$ ,  $r_D$ ,  $r_{eD}$ , and  $t_D$  for the constant- $\Delta p_w^*$  case are defined in Table 2.

The  $q_D^*$  under the constant- $\Delta p_w^*$  condition is expressed as:

$$q_D^* = - \frac{\partial p_D^*}{\partial r_D} \bigg|_{r_D=1}. \quad (22)$$

It is clear that  $q_D^*$  in Laplace space is the same as Equation (15):

$$\bar{q}_D^* = \frac{I_1(r_{eD} \sqrt{s})K_1(\sqrt{s}) - K_1(r_{eD} \sqrt{s})I_1(\sqrt{s})}{\sqrt{s}[I_0(\sqrt{s})K_1(r_{eD} \sqrt{s}) + K_0(\sqrt{s})I_1(r_{eD} \sqrt{s})]}. \quad (23)$$

**Table 2.** Definitions of pseudo-dimensionless and dimensionless variables for vertical wells.

Nomenclature	Constant- $\Delta p_w^*$ Case	Constant- $q^*$ Case
Pseudo-dimensionless pressure	$p_D^* = \frac{\Delta p^*}{\Delta p_w^*}$	$p_D^* = \frac{2\pi kh \Delta p^*}{q^* B \mu}$
Pseudo-dimensionless bottomhole pressure	$p_{wD}^* = 1$	$p_{wD}^* = \frac{2\pi kh \Delta p_w^*}{q^* B \mu}$
Dimensionless time	$t_D = \frac{kt}{\phi c_t \mu r_w^2}$	$t_D = \frac{kt}{\phi c_t \mu r_w^2}$
Dimensionless distance	$r_D = \frac{r}{r_w}, r_{eD} = \frac{r_e}{r_w}$	$r_D = \frac{r}{r_w}, r_{eD} = \frac{r_e}{r_w}$
Pseudo-dimensionless flow rate	$q_D^* = \frac{q^* B \mu}{2\pi kh \Delta p_w^*}$	$q_D^* = 1$

In the same way, if oil wells produce under the constant- $q^*$  condition, the seepage model of vertical wells in finite closed reservoirs based on the governing equation with the QGT is expressed as:

$$\frac{1}{r_D} \frac{\partial}{\partial r_D} \left( r_D \frac{\partial p_D^*}{\partial r_D} \right) = \frac{\partial p_D^*}{\partial t_D}, \quad (24)$$

$$p_D^*|_{t_D=0} = 0, \quad (25)$$

$$\left. \frac{\partial p_D^*}{\partial r_D} \right|_{r_D=r_{eD}} = 0, \quad (26)$$

$$\left( r_D \frac{\partial p_D^*}{\partial r_D} \right) \Big|_{r_D=1} = -1, \quad (27)$$

where  $p_D^*$ ,  $r_D$ ,  $r_{eD}$ , and  $t_D$  for the constant- $q^*$  case are defined in Table 2.

Similarly, it is obvious that the pseudo-dimensionless bottomhole pressure in Laplace space is the same as Equation (16):

$$\bar{p}_{wD}^* = \bar{p}_D^*|_{r_D=1} = \frac{K_1(r_{eD} \sqrt{s})I_0(\sqrt{s}) + I_1(r_{eD} \sqrt{s})K_0(\sqrt{s})}{s \sqrt{s}[K_1(\sqrt{s})I_1(r_{eD} \sqrt{s}) - I_1(\sqrt{s})K_1(r_{eD} \sqrt{s})]}. \quad (28)$$

In order to establish the relationship between  $q_D^*(t_D)$  under the constant- $\Delta p_w^*$  condition and  $p_{wD}^*(t_D)$  under the constant- $q^*$  condition, modified dimensionless material balance time is introduced as:

$$t_{cD}^* = \frac{1}{q_D^*} \int_0^{t_D} q_D^*(\tau) d\tau, \quad (29)$$

where  $t_{cD}^*$  is the modified dimensionless material balance time defined by  $t_{cD}^* = kt_c^* / (\phi c_t \mu r_w^2)$ ;  $t_c^*$  is the modified material balance time defined by:

$$t_c^* = \frac{1}{q \exp(-c_f \Delta p_w)} \int_0^t q(\tau) \exp(-c_f \Delta p_w) d\tau. \quad (30)$$

In the same way, the “ $q_D^*$  vs.  $t_{cD}^*$ ” curve for the constant- $\Delta p_w^*$  case almost coincided with the “ $1/p_{wD}^*$  vs.  $t_{cD}^*$ ” curve for the constant- $q^*$  case, both of which are the same as the “ $q_D$  vs.  $t_{cD}$ ” curve for the CPP

case and the “ $1/p_{wD}$  vs.  $t_{cD}$ ” curve for the CRP case, respectively. Similarly, the modified normalized rate function is introduced as:

$$\frac{q^*}{\Delta p_w^*} = \frac{q}{\Delta p_w} \frac{c_f \Delta p_w \exp(-c_f \Delta p_w)}{1 - \exp(-c_f \Delta p_w)}, \quad (31)$$

and then the curves of  $q^*/\Delta p_w^*$  versus  $t_c^*$  for the constant- $\Delta p_w^*$  and constant- $q^*$  cases are almost the same. Therefore, in order to take into account the effect of the QGT, modified normalized rate function (i.e., Equation (31)) and modified material balance time (i.e., Equation (30)) should be used to interpret production data.

### 3. Method for the Analysis of Production Data

The procedure for BPDA of production data of oil wells has been proposed by Blasingame and his co-workers [24] and widely used in practice from then on. To make a comparison between BPDA and PPDA, the step-by-step procedure for BPDA is listed in Appendix D. PPDA is established on the basis of the governing equation with the QGT and its procedure is presented as follows:

(1) Computation of modified material balance time

$$t_c^* = \frac{1}{q \exp(-c_f \Delta p_w)} \int_0^t q(\tau) \exp(-c_f \Delta p_w) d\tau, \quad (32)$$

where  $\Delta p_w = p_i - p_w$ .

(2) Computation of the modified normalized rate function

$$(q^*/\Delta p_w^*) = \frac{q^*}{\Delta p_w^*} = \frac{q}{\Delta p_w} \frac{c_f \Delta p_w \exp(-c_f \Delta p_w)}{1 - \exp(-c_f \Delta p_w)}. \quad (33)$$

(3) Computation of the modified normalized rate integral function

$$(q^*/\Delta p_w^*)_i = \frac{1}{t_c^*} \int_0^{t_c^*} \frac{q^*}{\Delta p_w^*} d\tau = \frac{1}{t_c^*} \int_0^{t_c^*} \frac{q}{\Delta p_w} \frac{c_f \Delta p_w \exp(-c_f \Delta p_w)}{1 - \exp(-c_f \Delta p_w)} d\tau. \quad (34)$$

(4) Computation of the modified normalized rate integral derivative function

$$(q^*/\Delta p_w^*)_{id} = -\frac{d(q^*/\Delta p_w^*)_i}{d \ln t_c^*} = -t_c^* \frac{d(q^*/\Delta p_w^*)_i}{dt_c^*}. \quad (35)$$

(5) Three log-log plots of  $(q^*/\Delta p_w^*)$  vs.  $t_c^*$ ,  $(q^*/\Delta p_w^*)_i$  vs.  $t_c^*$ , and  $(q^*/\Delta p_w^*)_{id}$  vs.  $t_c^*$  are plotted, respectively, and then matched on Blasingame type curves shown in Figure 3. The matched  $r_{eD}$  and the match point are recorded.

(6) The formation permeability can be obtained by

$$k = \frac{B\mu}{2\pi h} \frac{(q^*/\Delta p_w^*)_{MP}}{(q_{Dd})_{MP}} \left( \ln r_{eD} - \frac{1}{2} \right), \quad (36)$$

where  $(q^*/\Delta p_w^*)_{MP}$  is the real value of the match point, and  $(q_{Dd})_{MP}$  is the dimensionless value of the match point in Blasingame type curves.

(7) The drainage radius can be calculated by

$$r_e = \sqrt{\frac{\frac{B}{c_t} \frac{(t_c^*)_{MP}}{(t_{cDd})_{MP}} \frac{(q^*/\Delta p_w^*)_{MP}}{(q_{Dd})_{MP}}}{\pi h \phi}}. \quad (37)$$



(8) The effective wellbore radius and skin factor can be estimated by, respectively

$$r_{wa} = \frac{r_e}{r_{eD}}, \quad (38)$$

$$S = \ln\left(\frac{r_w}{r_{wa}}\right). \quad (39)$$

(9) The original oil-in-place can be calculated by

$$N = \frac{1}{c_t} \frac{(t_c^*)_{MP}}{(t_{cDd})_{MP}} \frac{(q^*/\Delta p_w^*)_{MP}}{(q_{Dd})_{MP}}. \quad (40)$$

It is found that both BPDA and PPDA are based on Blasingame type curves (see Figure 3), but there are some differences in the definitions of material balance time and normalized rate functions. PPDA can be reduced to BPDA if the value of  $c_f \Delta p_w$  infinitely approaches zero. The interpretation results of production data based on PPDA are consistent with material balance, and so we believe that the interpretation results based on PPDA are more accurate than these based on BPDA, especially when wells produce at a large drawdown pressure and fluid compressibility is large.

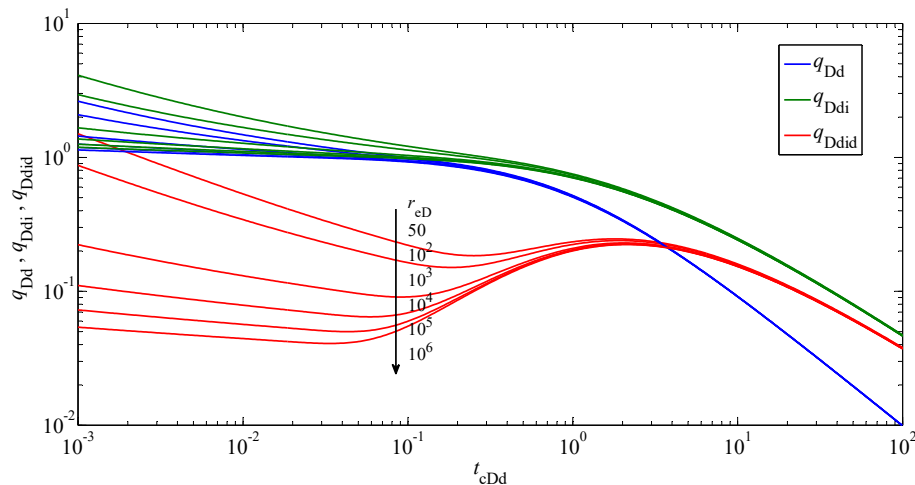


Figure 3. Blasingame type curves of vertical wells.

## 4. Validation and Application

### 4.1. Simulated Case Validation

In this section, the numerical model based on the governing equation with the QGT (see Appendix E) was employed to model performances of wells under different production conditions. The input parameters for the simulated cases, including CPP cases, CRP cases, and variable-rate/pressure cases, are listed in Table 3. Because the rock compressibility is very small compared with the fluid compressibility, the value of the total compressibility  $c_t$  was set as the value of the fluid compressibility  $c_f$  in the simulated cases. The generated production data by the numerical model was employed to conduct production decline analysis. Matched results of PPDA were validated by the input reservoir parameters and compared with the matched results of BPDA.

**Table 3.** Data used for the simulated cases.

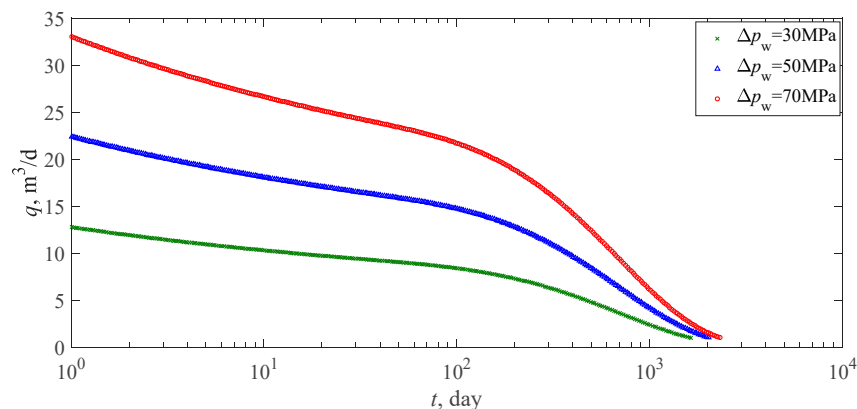
Parameter	Value		
	CPP Case	CRP Case	Variable-Rate/Pressure Case
Permeability, $k$ , mD	5	5	5
Volume factor, $B$ , $\text{m}^3/\text{m}^3$	1.1	1.1	1.1
Viscosity, $\mu$ , $\text{mPa} \cdot \text{s}$	20	20	20
Reservoir thickness, $h$ , m	15	15	15
Porosity, $\phi$	0.1	0.1	0.1
Oil compressibility, $c_f$ , $\text{MPa}^{-1}$	$50 \times 10^{-4}$	$50 \times 10^{-4}$	$50 \times 10^{-4}$
Wellbore radius, $r_w$ , m	0.1	0.1	0.1
Initial reservoir pressure, $p_i$ , MPa	80	80	80
Drainage radius, $r_e$ , m	100	10	100

#### 4.1.1. CPP Cases

The CPP cases were chosen as those of wells producing at a large drawdown pressure  $\Delta p_w$  (i.e.,  $\Delta p_w = 30$  MPa, 50 MPa, and 70 MPa) so as to highlight the effect of the QGT. The CPP cases with  $\Delta p_w = 30$  MPa, 50 MPa, and 70 MPa were simulated by the numerical model with the input parameters listed in Table 3, respectively. The production data for the CPP cases was obtained and the corresponding flow rates are shown in Figure 4. Normalized rate functions (i.e.,  $(q/\Delta p_w)$ ,  $(q/\Delta p_w)_i$ ,  $(q/\Delta p_w)_{id}$ ) and material balance time  $t_c$  were prepared for BPDA. Similarly, modified normalized rate functions (i.e.,  $(q^*/\Delta p_w^*)$ ,  $(q^*/\Delta p_w^*)_i$ ,  $(q^*/\Delta p_w^*)_{id}$ ) and modified material balance time  $t_c^*$  were calculated for PPDA. The plots of normalized rate functions (i.e.,  $(q/\Delta p_w)$ ,  $(q/\Delta p_w)_i$ ,  $(q/\Delta p_w)_{id}$ ) versus material balance time  $t_c$ , together with the plots of modified normalized rate functions (i.e.,  $(q^*/\Delta p_w^*)$ ,  $(q^*/\Delta p_w^*)_i$ ,  $(q^*/\Delta p_w^*)_{id}$ ) versus modified material balance time  $t_c^*$ , are shown in Figures 5–7 for CPP cases, respectively. Then, both normalized-rate-function plots and modified-normalized-rate-function plots were matched on Blasingame type curves as shown in Figures 8–10. It was observed from Figures 8–10 that excellent type curve matches were obtained for the three CPP cases. The matched dimensionless drainage radius  $r_{eD}$  and the match point were recorded, which were used to estimate reservoir parameters. The estimated results obtained with BPDA and PPDA are listed in Table 4 and relative differences between the actual values and estimated values are shown in Table 5. The relative difference between the actual value and estimated value is defined by:

$$\delta = \frac{|\psi_{av} - \psi_{ev}|}{\psi_{av}} \times 100\%, \quad (41)$$

where  $\delta$  is the relative difference between the actual value and estimated value;  $\psi_{av}$ ,  $\psi_{ev}$  are the actual value and estimated value of a parameter, respectively.

**Figure 4.** Production data for CPP cases with different values of drawdown pressure  $\Delta p_w$ .

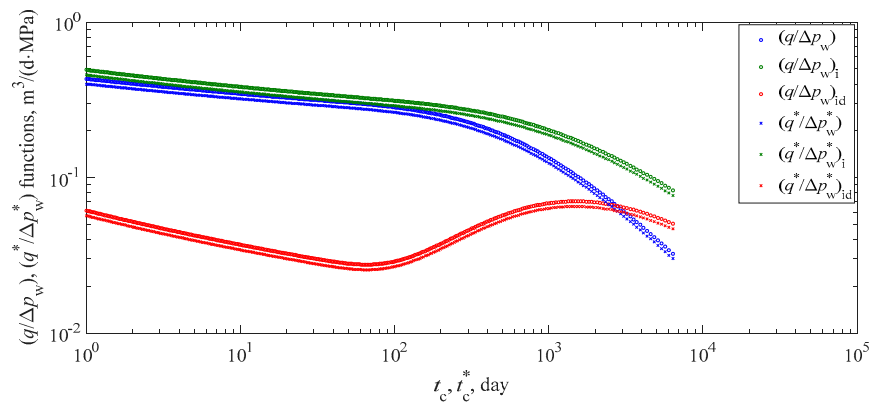


Figure 5. Normalized rate functions and modified normalized rate functions for CPP case of  $\Delta p_w = 30$  MPa.

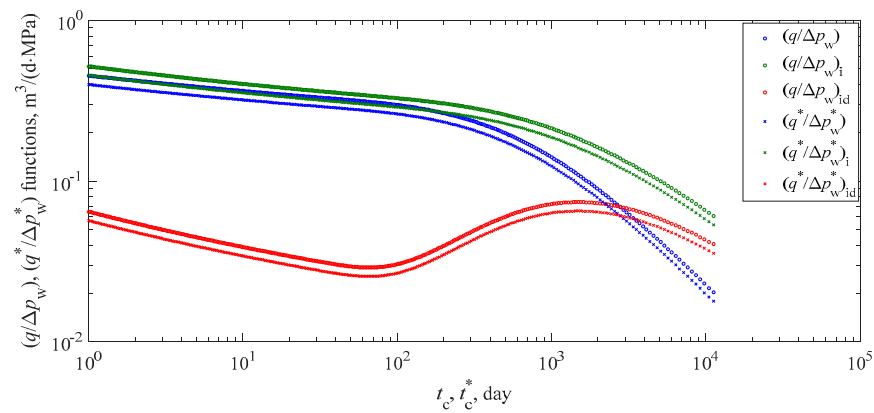


Figure 6. Normalized rate functions and modified normalized rate functions for CPP case of  $\Delta p_w = 50$  MPa.

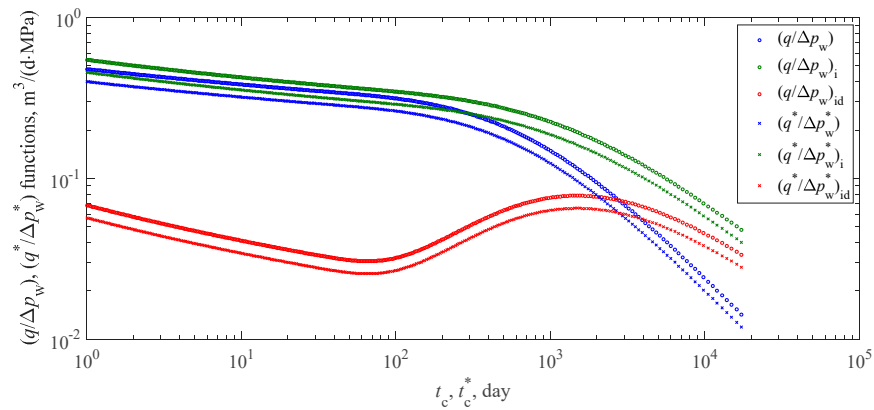
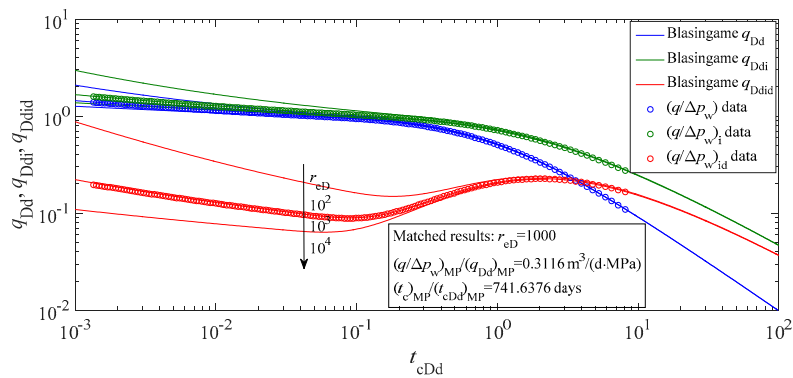
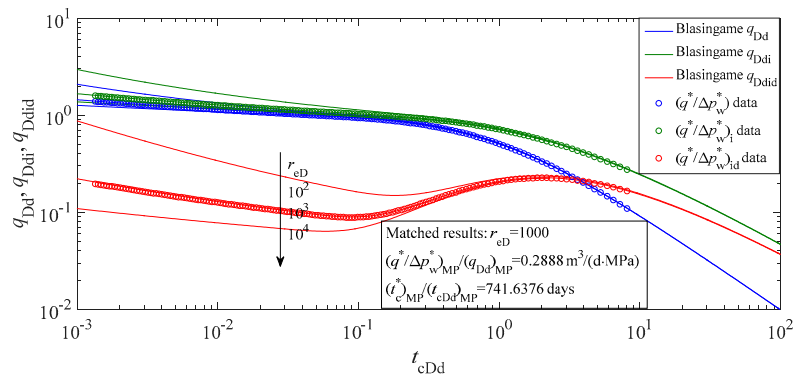


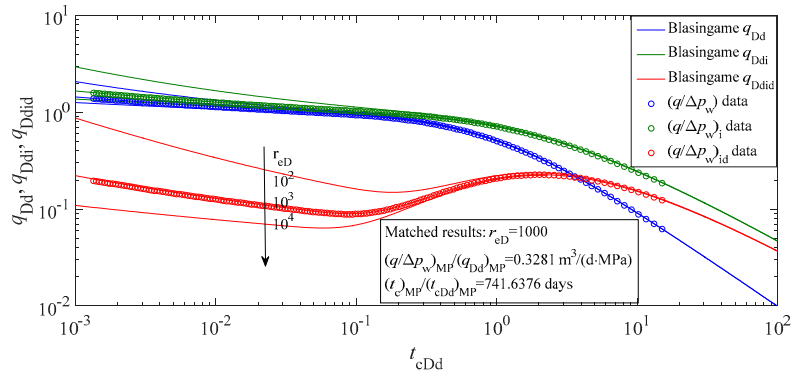
Figure 7. Normalized rate functions and modified normalized rate functions for CPP case of  $\Delta p_w = 70$  MPa.



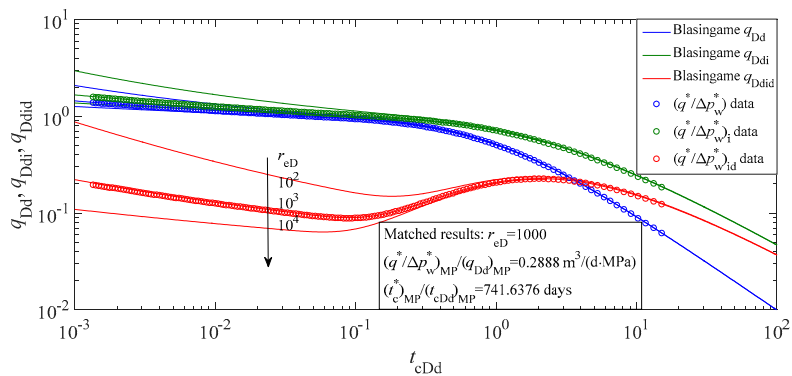
(a) Match of production data based on Blasingame production decline analysis



(b) Match of production data based on our proposed production decline analysis

**Figure 8.** Match of production data for CPP case of  $\Delta p_w = 30$  MPa.

(a) Match of production data based on Blasingame production decline analysis



(b) Match of production data based on our proposed production decline analysis

**Figure 9.** Match of production data for CPP case of  $\Delta p_w = 50$  MPa.

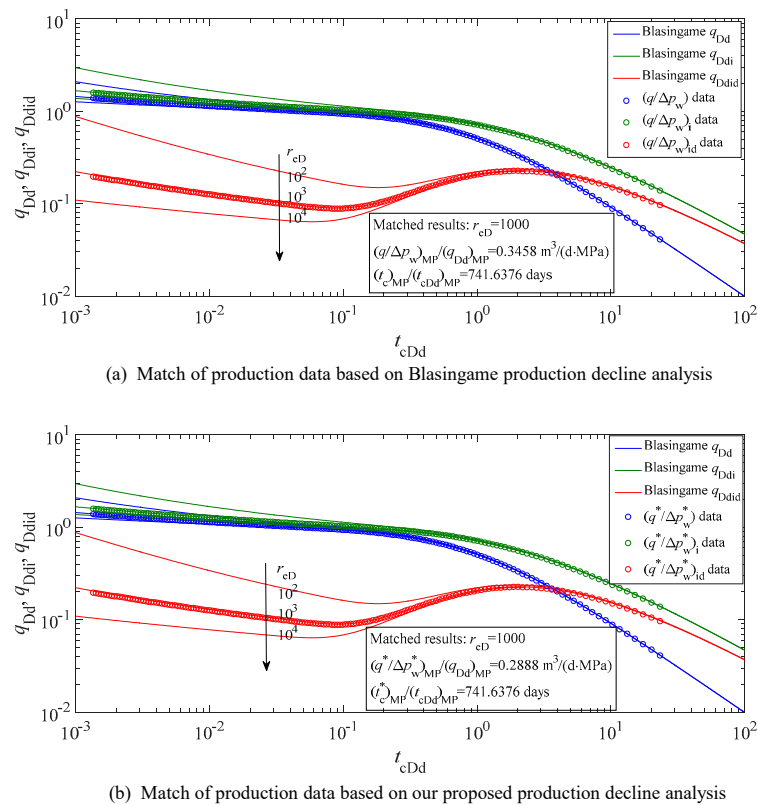


**Figure 10.** Match of production data for CPP case of  $\Delta p_w = 70$  MPa.

**Table 4.** Comparison between the results obtained by BPDA and PPDA for CPP cases.

Parameter	Actual Value	Production Decline Analysis Result					
		$\Delta p_w = 30$ MPa		$\Delta p_w = 50$ MPa		$\Delta p_w = 70$ MPa	
		BPDA	PPDA	BPDA	PPDA	BPDA	PPDA
$k$ , mD	5	5.395	5	5.681	5	5.987	5
$r_e$ , m	100	103.870	100	106.588	100	109.423	100
$N$ , $10^4 \text{m}^3$	4.284	4.622	4.284	4.867	4.284	5.129	4.284
$S$	0	−0.038	0	−0.064	0	−0.090	0

**Table 5.** Relative differences between the actual values and estimated values for CPP cases.

Parameter	Relative Difference $\delta$ (%)					
	$\Delta p_w = 30$ MPa		$\Delta p_w = 50$ MPa		$\Delta p_w = 70$ MPa	
	BPDA	PPDA	BPDA	PPDA	BPDA	PPDA
$k$ , mD	7.90	0	13.62	0	19.74	0
$r_e$ , m	3.87	0	6.59	0	9.42	0
$N$ , $10^4 \text{m}^3$	7.89	0	13.61	0	19.72	0
$S$	−	−	−	−	−	−

It was found that the values of parameters estimated by BPDA were different from the actual values (i.e., the data input to the numerical model) for CPP cases, while the results estimated by PPDA were the same as the data input to the numerical model, verifying PPDA for CPP cases. It is interesting that both the permeability and original oil-in-place estimated by BPDA are larger than the actual values, and the relative difference between the actual value and estimated value increases with increasing the drawdown pressure for CPP cases, indicating that BPDA overestimates reservoir properties and original oil-in-place, especially when wells produce at a large drawdown pressure. This is because

the production data is generated by the numerical model on the basis of the governing equation with the QGT. The existence of the QGT enhances the capacity of fluid flow [34], so a larger permeability is estimated by BPDA, which is established on the basis of the conventional governing equation without the QGT. If the estimated permeability becomes larger, the pressure wave can spread over a longer distance within the same time, and thus the estimated drainage radius and original oil-in-place become larger. According to the comparison between BPDA and PPDA, as the drawdown pressure  $\Delta p_w$  increases, the value of  $c_f \Delta p_w$  becomes larger, which results in a greater error in the interpretation of production data.

#### 4.1.2. CRP Cases

The CRP cases were chosen as those of wells producing at a large flow rate  $q$  (i.e.,  $q = 10 \text{ m}^3/\text{d}$ ,  $20 \text{ m}^3/\text{d}$ , and  $30 \text{ m}^3/\text{d}$ ) so as to highlight the effect of the QGT. The CRP cases with  $10 \text{ m}^3/\text{d}$ ,  $20 \text{ m}^3/\text{d}$ , and  $30 \text{ m}^3/\text{d}$  were considered here and the  $\Delta p_w$  responses for the three cases were obtained by inputting the constant rates into the numerical model (see Figure 11). The basic input parameters for CRP cases are listed in Table 3. On the basis of the simulated production data by the numerical model, “ $(q/\Delta p_w)$  vs.  $t_c$ ”, “ $(q/\Delta p_w)_i$  vs.  $t_c$ ”, and “ $(q/\Delta p_w)_{id}$  vs.  $t_c$ ” for BPDA and “ $(q^*/\Delta p_w^*)$  vs.  $t_c^*$ ”, “ $(q^*/\Delta p_w^*)_i$  vs.  $t_c^*$ ”, and “ $(q^*/\Delta p_w^*)_{id}$  vs.  $t_c^*$ ” for PPDA were obtained (see Figures 12–14). Following the procedures for BPDA and PPDA, the matches of the normalized rate functions and modified normalized rate functions on Blasingsame type curves for the three CRP cases were conducted and shown in Figures 15–17, from which we can see that good type curve matches were obtained for all the three cases. The matched results obtained by BPDA and PPDA are listed in Table 6 and relative differences between the actual values and estimated values are shown in Table 7. It is obvious that the results estimated by BPDA are different from the actual values (i.e., the data input to the numerical model) for CRP cases, while the results estimated by PPDA are the same as the data input to the numerical model, verifying PPDA for CRP cases. It is found that both the permeability and original oil-in-place estimated by BPDA are larger than the actual values, and the relative difference between the actual value and estimated value increases with an increase in the flow rate for CRP cases, indicating that reservoir properties and original oil-in-place obtained by BPDA are also overestimated especially when wells produce at large flow rates. The reason is similar to that for CPP cases. As the flow rate is enhanced, the drawdown pressure  $\Delta p_w$  of wells should increase to maintain the flow rate, which leads to a larger value of  $c_f \Delta p_w$ . Therefore, there is a larger error in the interpretation of production data based on BPDA when the flow rate of wells becomes larger.

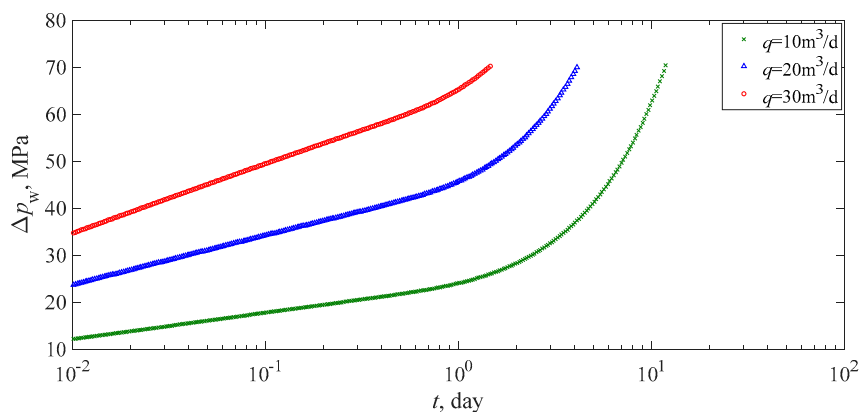
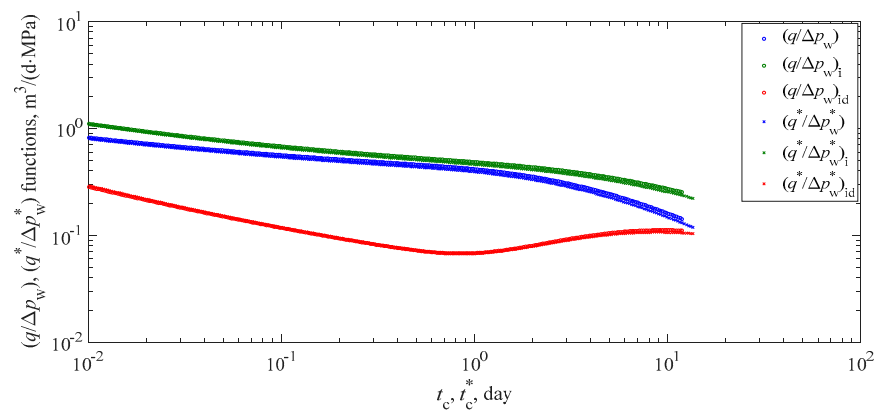
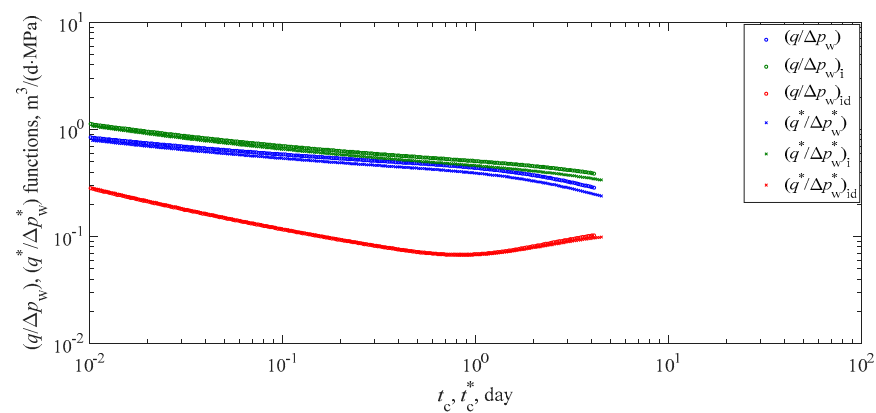


Figure 11. Production data for CRP cases with different values of flow rate  $q$ .



**Figure 12.** Normalized rate functions and modified normalized rate functions for CRP case of  $q = 10 \text{ m}^3/\text{d}$ .



**Figure 13.** Normalized rate functions and modified normalized rate functions for CRP case of  $q = 20 \text{ m}^3/\text{d}$ .

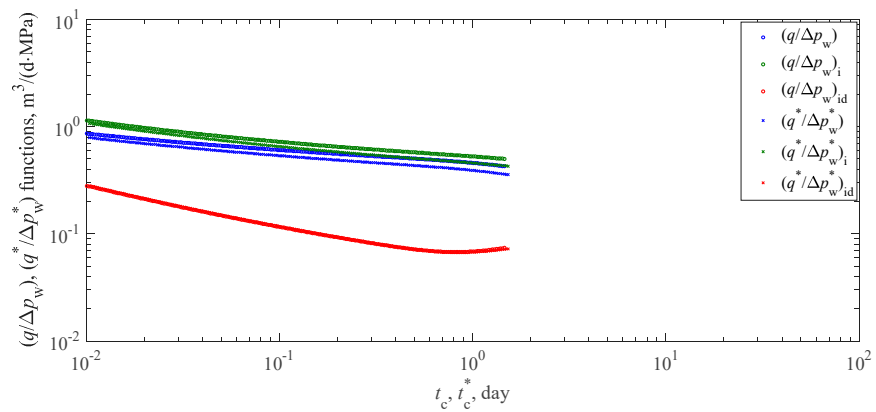
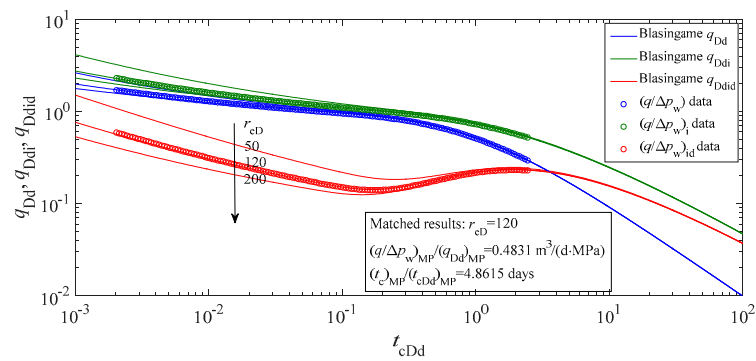
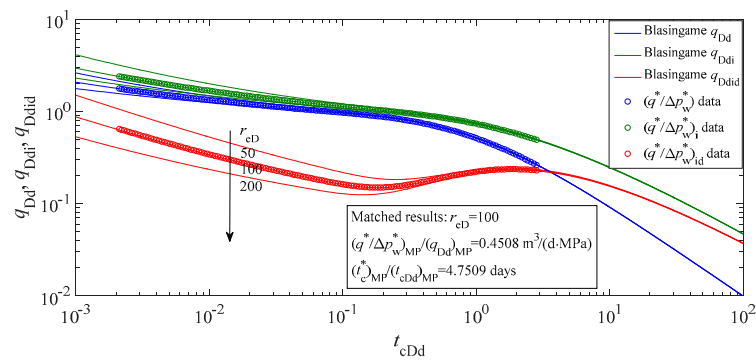


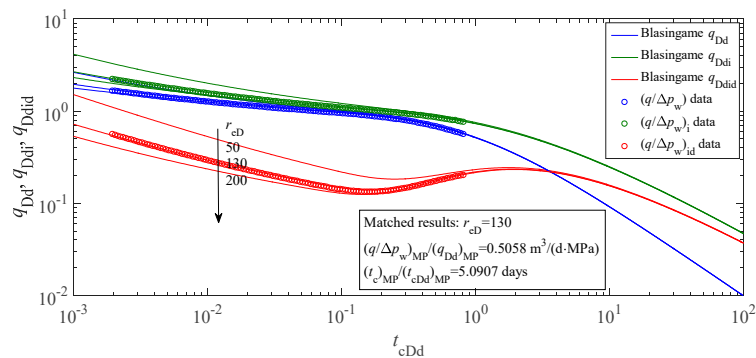
**Figure 14.** Normalized rate functions and modified normalized rate functions for CRP case of  $q = 30 \text{ m}^3/\text{d}$ .



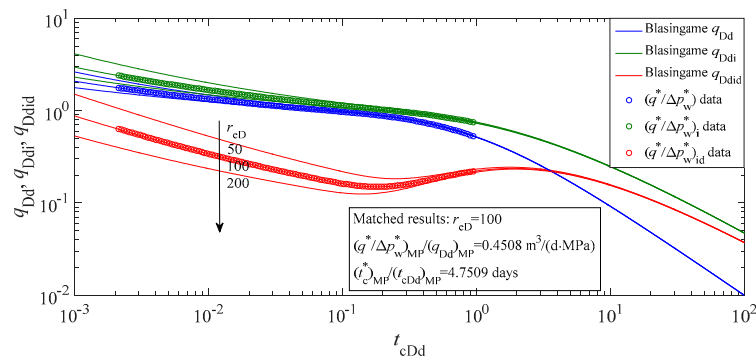
(a) Match of production data based on Blasingame production decline analysis



(b) Match of production data based on our proposed production decline analysis

**Figure 15.** Match of production data for CRP case of  $q = 10 \text{ m}^3/\text{d}$ .

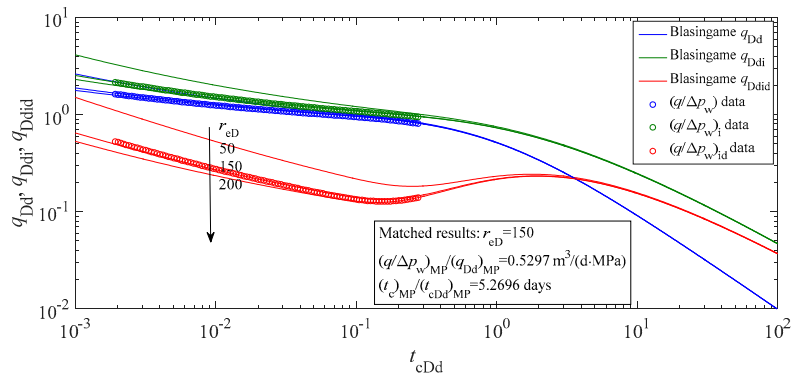
(a) Match of production data based on Blasingame production decline analysis



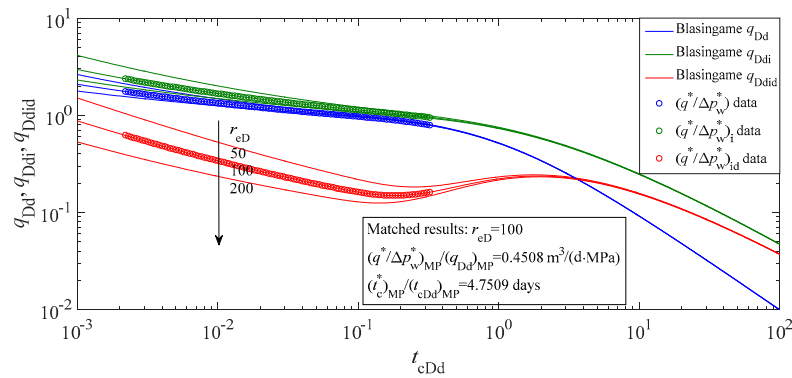
(b) Match of production data based on our proposed production decline analysis

**Figure 16.** Match of production data for CRP case of  $q = 20 \text{ m}^3/\text{d}$ .





(a) Match of production data based on Blasingame production decline analysis



(b) Match of production data based on our proposed production decline analysis

**Figure 17.** Match of production data for CRP case of  $q = 30 \text{ m}^3/\text{d}$ .**Table 6.** Comparison between the results obtained by BPDA and PPDA for CRP cases.

Parameter	Actual Value	Production Decline Analysis Result					
		$q = 10 \text{ m}^3/\text{d}$		$q = 20 \text{ m}^3/\text{d}$		$q = 30 \text{ m}^3/\text{d}$	
		BPDA	PPDA	BPDA	PPDA	BPDA	PPDA
$k$ , mD	5	5.596	5	5.969	5	6.455	5
$r_e$ , m	10	10.471	10	10.964	10	11.415	10
$N$ , $10^4 \text{ m}^3$	0.0428	0.0470	0.0428	0.0515	0.0428	0.0558	0.0428
$S$	0	0.136	0	0.1703	0	0.273	0

**Table 7.** Relative differences between the actual values and estimated values for CRP cases.

Parameter	Relative Difference $\delta$ (%)					
	$q = 10 \text{ m}^3/\text{d}$		$q = 20 \text{ m}^3/\text{d}$		$q = 30 \text{ m}^3/\text{d}$	
	BPDA	PPDA	BPDA	PPDA	BPDA	PPDA
$k$ , mD	11.92	0	19.38	0	29.10	0
$r_e$ , m	4.71	0	9.64	0	14.15	0
$N$ , $10^4 \text{ m}^3$	9.81	0	20.33	0	30.37	0
$S$	-	-	-	-	-	-

#### 4.1.3. Variable-Rate/Pressure Cases

As most wells produce at a variable rate/pressure rather than a constant flow rate or a constant pressure in practice, we focus on the applicability of PPDA for variable-rate/pressure cases in this subsection. Here we considered two common types of variable-rate/pressure production, which were the case of first producing at a constant rate and then producing at a constant pressure (i.e., Case 1–3

shown in Table 8) and the case of multiple rate/pressure changes (i.e., Case 4 shown in Table 9). The two types of variable-rate/pressure production are close to actual performances of wells and can be considered representative of actual production histories of wells. In order to highlight the effect of the QGT, the cases were also chosen as those of wells producing at large drawdown pressures or large flow rates. Table 8 shows the production histories of the cases for vertical wells first producing at a constant rate and then producing at a constant pressure. Vertical wells first produce at the constant rate  $q$  until the drawdown pressure reaches a specified value  $\Delta p_w$ , and then vertical wells produce at the constant drawdown pressure  $\Delta p_w$ . Table 9 shows the production history of the case for vertical wells producing at multiple rate/pressure changes. The production data for the four cases, which were obtained by inputting the production histories into the numerical model, are shown in Figures 18 and 19. The basic input parameters for the variable-rate/pressure cases are listed in Table 3.  $“(q/\Delta p_w) \text{ vs. } t_c”$ ,  $“(q/\Delta p_w)_i \text{ vs. } t_c”$ , and  $“(q/\Delta p_w)_{id} \text{ vs. } t_c”$  for BPDA and  $“(q^*/\Delta p_w^*) \text{ vs. } t_c”$ ,  $“(q^*/\Delta p_w^*)_i \text{ vs. } t_c”$ , and  $“(q^*/\Delta p_w^*)_{id} \text{ vs. } t_c”$  for PPDA were calculated by the simulated production data, which are shown in Figures 20–23 for the four cases, respectively. Excellent matches of the normalized rate functions and modified normalized rate functions on Blasingame type curves for the four cases were obtained, which are shown in Figures 24–27. The matched results obtained by BPDA and PPDA are listed in Table 10 and relative differences between the actual values and estimated values are shown in Table 11. It is seen that the formation permeability, drainage radius, original oil-in-place, and skin factor estimated by BPDA are also different from the actual values (i.e., the data input to the numerical model) for variable-rate/pressure cases, while the results estimated by PPDA are also the same as the data input to the numerical model, verifying PPDA for variable-rate/pressure cases. Furthermore, it is also found that BPDA overestimates the permeability and original oil-in-place for variable-rate/pressure cases, especially when wells produce at large drawdown pressures or large flow rates.

**Table 8.** Production histories of cases for a vertical well first producing at a constant rate and then producing at a constant pressure.

Case	Constant Rate Production	Constant Pressure Production
	$q, \text{ m}^3/\text{d}$	$\Delta p_w, \text{ MPa}$
Case 1	10	30
Case 2	10	70
Case 3	20	70

**Table 9.** Production history of Case 4 for a vertical well producing at multiple rate/pressure changes.

$t, \text{ day}$	$q, \text{ m}^3/\text{d}$	$\Delta p_w, \text{ MPa}$
0–50	10	variable
51–100	14	variable
101–150	12	variable
151–200	16	variable
201–350	variable	60
351–700	variable	50
701–1500	variable	55

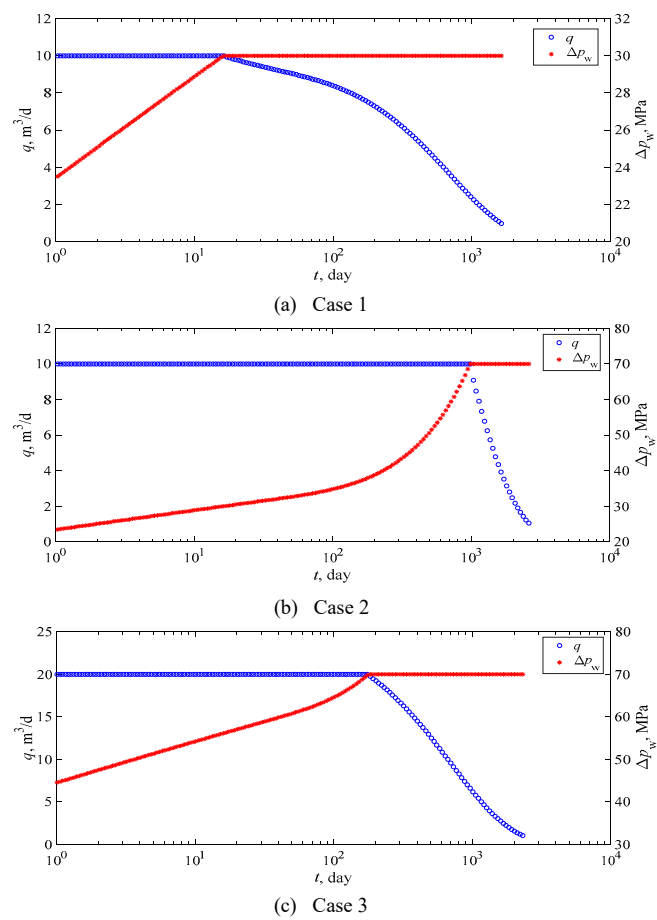


**Figure 18.** Production data for Cases 1–3 with variable rate and pressure.

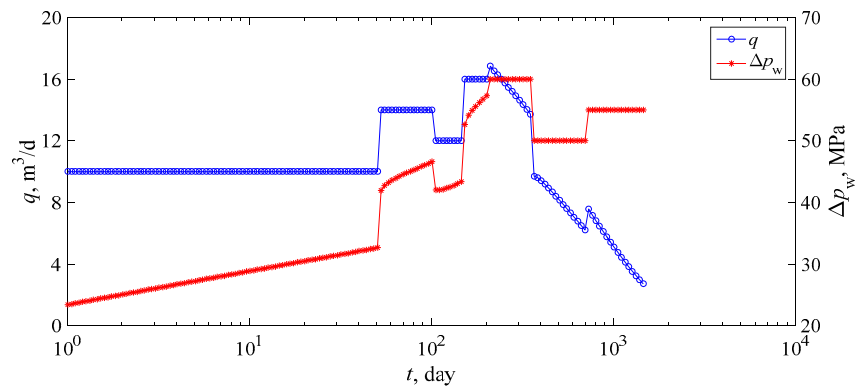


**Figure 19.** Production data for Case 4 with variable rate and pressure.

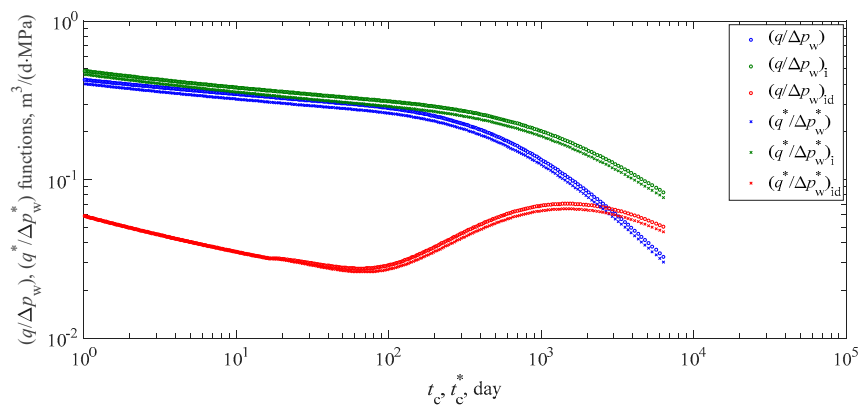


**Figure 20.** Normalized rate functions and modified normalized rate functions for Case 1.

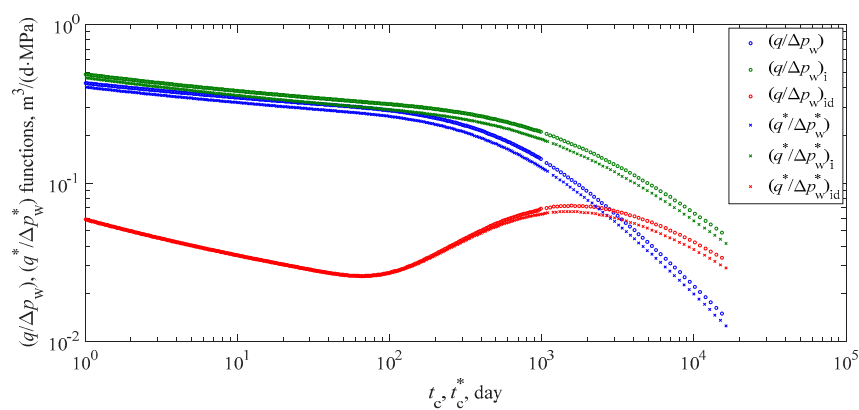


**Figure 21.** Normalized rate functions and modified normalized rate functions for Case 2.

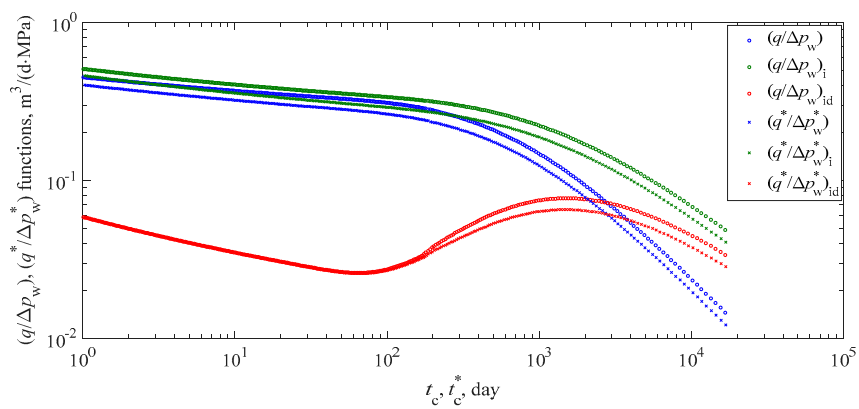


**Figure 22.** Normalized rate functions and modified normalized rate functions for Case 3.

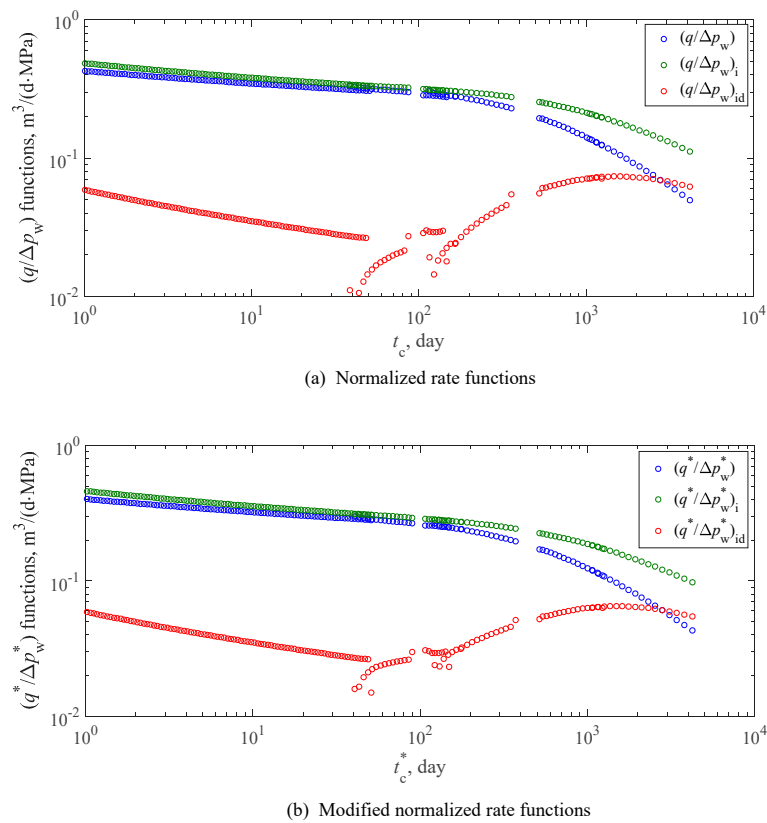


**Figure 23.** Normalized rate functions and modified normalized rate functions for Case 4.

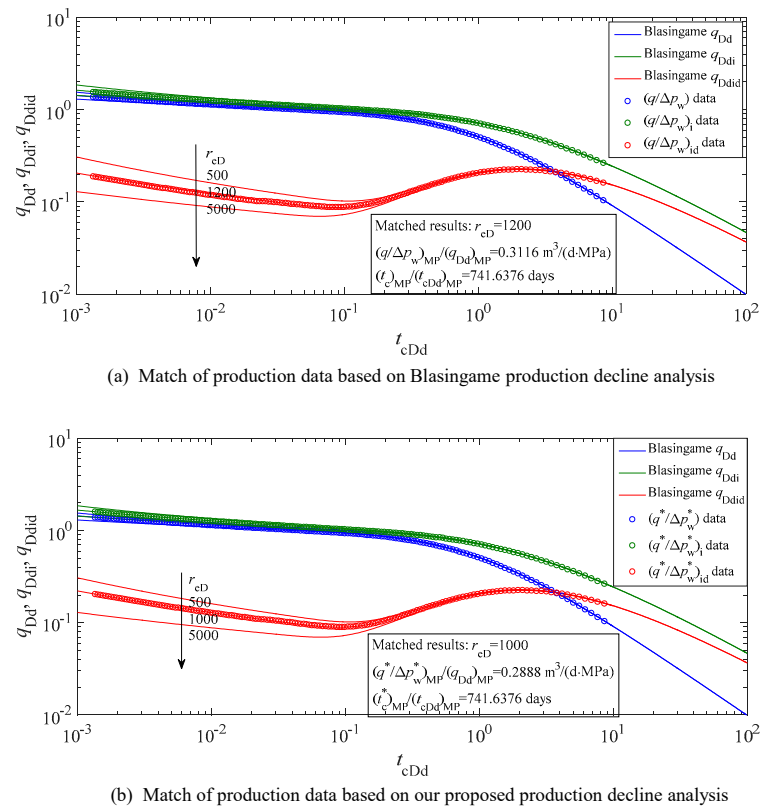
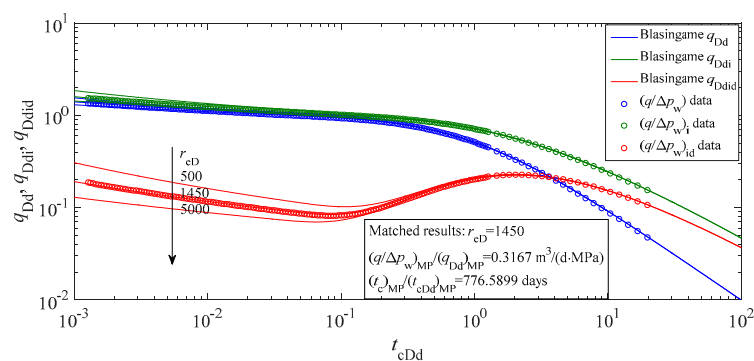
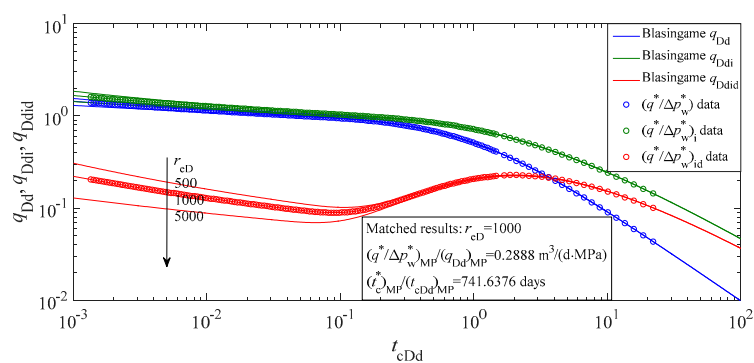


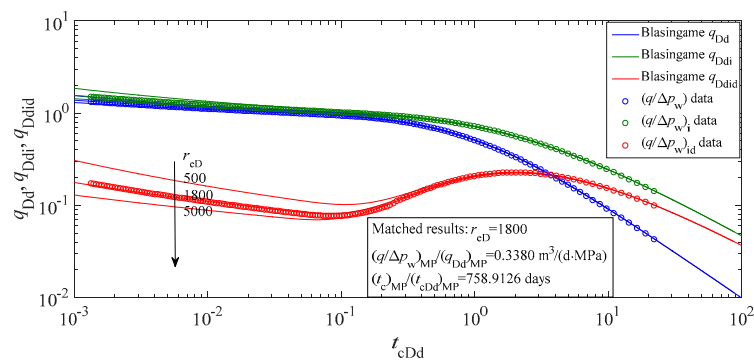
**Figure 24.** Match of production data for Case 1.



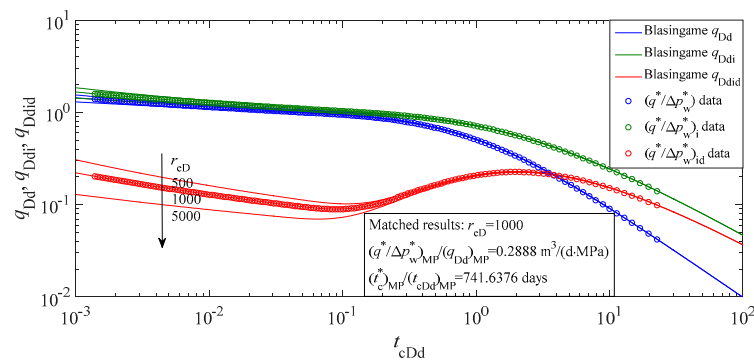
(a) Match of production data based on Blasingame production decline analysis



(b) Match of production data based on our proposed production decline analysis

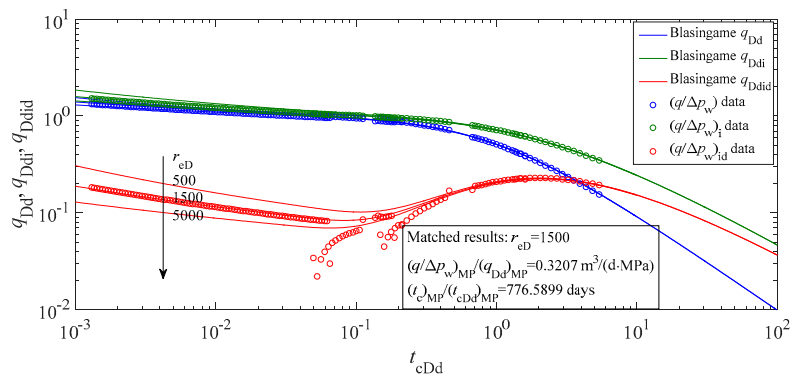
**Figure 25.** Match of production data for Case 2.

(a) Match of production data based on Blasingame production decline analysis

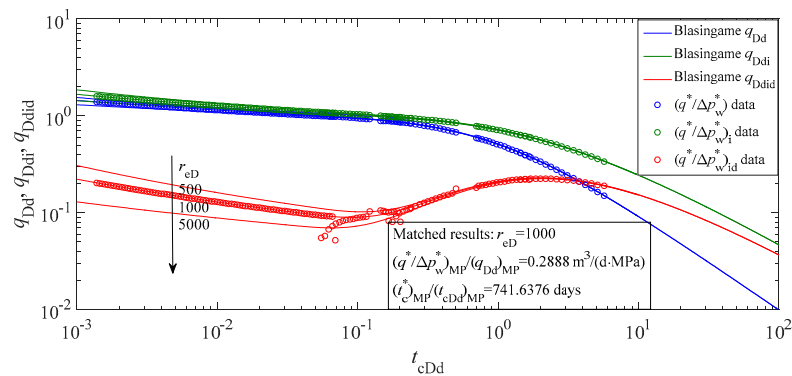


(b) Match of production data based on our proposed production decline analysis

**Figure 26.** Match of production data for Case 3.



(a) Match of production data based on Blasingame production decline analysis



(b) Match of production data based on our proposed production decline analysis

Figure 27. Match of production data for Case 4.

Table 10. Comparison between the results obtained by BPDA and PPDA for variable-rate/pressure cases.

Parameter	Actual Value	Production Decline Analysis Result							
		Case 1		Case 2		Case 3		Case 4	
		BPDA	PPDA	BPDA	PPDA	BPDA	PPDA	BPDA	PPDA
$k$ , mD	5	5.548	5	5.800	5	6.387	5	5.903	5
$r_e$ , m	100	103.870	100	107.152	100	109.423	100	107.822	100
$N$ , $10^4\text{m}^3$	4.284	4.622	4.284	4.919	4.284	5.129	4.284	4.980	4.284
$S$	0	0.144	0	0.303	0	0.498	0	0.330	0

Table 11. Relative differences between the actual values and estimated values for variable-rate/pressure cases.

Parameter	Relative Difference $\delta$ (%)							
	Case 1		Case 2		Case 3		Case 4	
	BPDA	PPDA	BPDA	PPDA	BPDA	PPDA	BPDA	PPDA
$k$ , mD	10.96	0	16.00	0	27.74	0	18.06	0
$r_e$ , m	3.87	0	7.15	0	9.42	0	7.82	0
$N$ , $10^4\text{m}^3$	7.89	0	14.82	0	19.72	0	16.25	0
$S$	-	-	-	-	-	-	-	-

#### 4.1.4. Discussion of Validation

The simulated cases in a variety of production scenarios provide a good test of the validity of PPDA. Based on the above analysis, it was found that the results of PPDA are the same as the data input to the numerical model for all the cases including CPP cases, CRP cases, and variable-rate/pressure

cases. Because BPDA is inconsistent with material balance, BPDA overestimates the permeability and original oil-in-place for all the cases, especially when wells produce at large drawdown pressures or large flow rates.

Recent studies have demonstrated that the ultra-deep reservoirs (a depth greater than 4500 m) may contain abundant oil and gas resources [41]. In the past decades, many ultra-deep, high-pressure reservoirs have been discovered and developed in various parts of the world [36]. Commercial development of these reservoirs may require producing wells with large drawdown pressures. Furthermore, in order to realize fast cost recovery and obtain better economic benefits, the policy of “fewer wells with higher oil rate, large drawdown pressure” has been employed to develop various reservoirs, especially the offshore oilfields, the oilfields with contract term and investment risks, and so on [42]. Therefore, it is better to make the interpretation of production data considering the effect of the QGT in practice. Compared with BPDA, PPDA can be used to more accurately interpret production data with little increase in computation time. Therefore, PPDA provides a better way to interpret production data.

#### 4.2. Field Application

A field case was employed to show the proposed method can be used in practice. Well XHa located in Halahatang oilfield in Tarim Basin of China is a flowing oil well. The production data for Well XHa under the flush stage is shown in Figure 28. Basic parameters of Well XHa are listed in Table 12. Normalized rate functions and modified normalized rate functions for Well XHa are shown in Figure 29. The matches of the normalized rate functions and modified normalized rate functions on Blasingame type curves are conducted and shown in Figure 30. The matched results obtained by BPDA and PPDA are listed in Table 13, from which we can see that neglecting the effect of the QGT results in the overestimation of the permeability and original oil-in-place for BPDA. Furthermore, the index of correlation ( $R^2$ ) is introduced to quantify the fit between the test data and the computed data for normalized rate function ( $q/\Delta p_w$ ) and modified normalized rate function ( $q^*/\Delta p_w^*$ ), respectively. It is seen from Table 13 that the index of correlation ( $R^2$ ) is 0.9895 for BPDA and 0.9932 for PPDA, which shows the test data matches well with the computed data for both BPDA and PPDA.

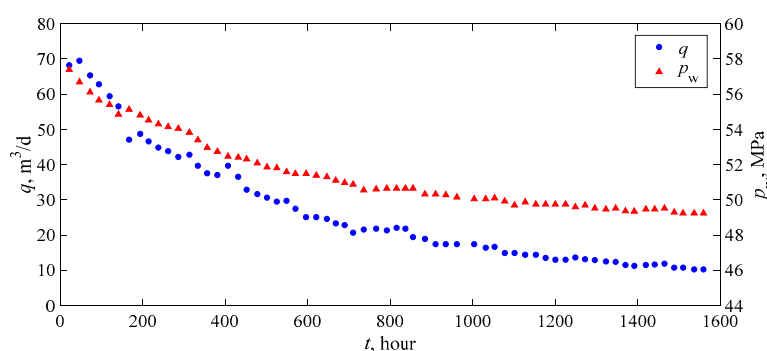


Figure 28. Production data for Well XHa.

Table 12. Basic parameters of Well XHa.

Parameter	Value
Volume factor, $B$ , $\text{m}^3/\text{m}^3$	1.18
Viscosity, $\mu$ , $\text{mPa} \cdot \text{s}$	5.35
Reservoir thickness, $h$ , m	12
Porosity, $\phi$	0.08
Oil compressibility, $c_f$ , $\text{MPa}^{-1}$	$56 \times 10^{-4}$
Total compressibility, $c_t$ , $\text{MPa}^{-1}$	$58 \times 10^{-4}$
Wellbore radius, $r_w$ , m	0.06
Initial reservoir pressure, $p_i$ , MPa	77.6



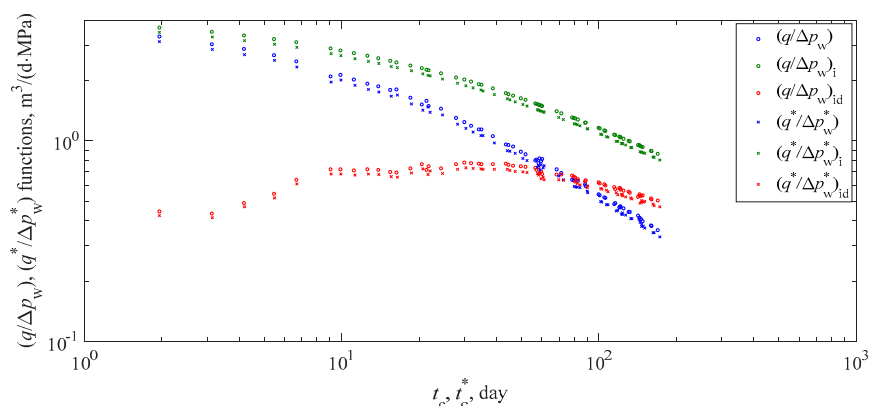
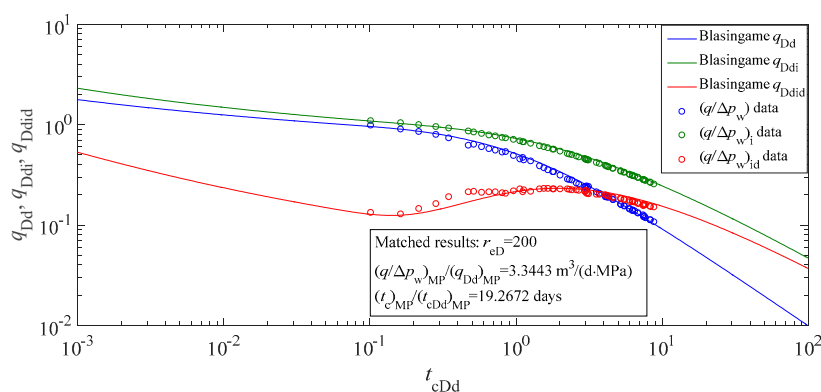
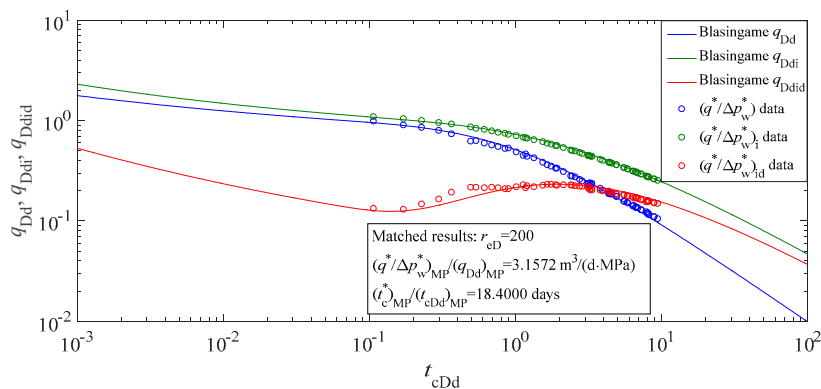


Figure 29. Normalized rate functions and modified normalized rate functions for Well XHa.



(a) Match of production data based on Blasingame production decline analysis



(b) Match of production data based on our proposed production decline analysis

Figure 30. Match of production data for Well XHa.

Table 13. Comparison between the results obtained by BPDA and PPDA for Well XHa.

Index of Correlation ( $R^2$ )		Parameter	Production Decline Analysis Result		Relative Difference (%)
BPDA	PPDA		BPDA	PPDA	
0.9895	0.9932	$k$ , mD	15.550	14.680	5.93
		$r_e$ , m	65.928	62.599	5.32
		$N$ , $10^4$ m <sup>3</sup>	1.111	1.002	10.88
		$S$	−1.704	−1.652	3.15

## 5. Conclusions

In this work, we modified material balance time and normalized rate functions and hence improved BPDA, which neglected the impact of the QGT. The step-by-step procedure for PPDA was presented

and compared with that for BPDA. The simulated cases for various production scenarios were used to validate PPDA, and a field case was employed to test its applicability in practice. The errors in the interpretation of production data based on BPDA were analyzed in detail. Several conclusions are listed as follows:

- (1) Both BPDA and PPDA are implemented by matching corresponding normalized rate functions on Blasingame type curves. The main differences between them are the definitions of material balance time and normalized rate functions. If the value of  $c_f \Delta p_w$  infinitely approaches zero, PPDA is simplified as BPDA. Therefore, interpreting production data based on PPDA is relatively straightforward.
- (2) PPDA can predict better estimates of reservoir properties and original oil-in-place for oil reservoirs compared to BPDA. The latter overestimates permeability and original oil-in-place, especially when wells produce at large drawdown pressures or large flow rates.
- (3) Fluid flow in actual reservoirs is consistent with material balance, and thus compared with BPDA, PPDA can be used to more accurately interpret production data with little increase in computation time.

**Author Contributions:** Conceptualization, J.R.; Formal analysis, J.R.; Funding acquisition, J.R.; Investigation, J.R. and Q.Z.; Methodology, J.R.; Project administration, J.R.; Supervision, J.R.; Validation, Q.Z.; Visualization, C.Z.; Writing—original draft, J.R.; Writing—review & editing, Q.Z.

**Funding:** We acknowledge the support provided by Open Fund of State Key Laboratory of Oil and Gas Reservoir Geology and Exploitation (PLN201627), the Natural Science Project of Sichuan Province Department of Education (No. 17ZA0425), the Scientific Research Starting Project of SWPU (No. 2017QHZ031).

**Conflicts of Interest:** The authors declare no conflict of interest.

## Nomenclature

### Roman Symbols

$B$	volume factor, $\text{m}^3/\text{m}^3$
$c_f$	fluid compressibility, $\text{Pa}^{-1}$
$c_r$	rock compressibility, $\text{Pa}^{-1}$
$c_t$	total compressibility, $\text{Pa}^{-1}$
$h$	formation thickness, m
$I_0(x)$	modified Bessel function of the first kind, zero order
$I_1(x)$	modified Bessel function of the first kind, first order
$K_0(x)$	modified Bessel function of the second kind, zero order
$K_1(x)$	modified Bessel function of the second kind, first order
$k$	permeability, $\text{m}^2$
$M$	number of the space grid
$N$	original oil-in-place, $\text{m}^3$
$p$	formation pressure, Pa
$p_D^*$	pseudo-dimensionless pressure, defined in Table 2
$p_i$	initial formation pressure, Pa
$p_w$	bottomhole pressure, Pa
$p_{wD}^*$	pseudo-dimensionless bottomhole pressure, defined in Table 2
$q$	flow rate, $\text{m}^3/\text{s}$
$q^*$	transformed flow rate, defined in Equation (12)
$q_D^*$	pseudo-dimensionless flow rate, defined in Table 2
$r$	radial distance, m
$r_e$	outer boundary radius, m
$r_w$	wellbore radius, m
$r_{wa}$	effective wellbore radius, m

*Roman Symbols*

$s$	Laplace transform variable
$S$	skin factor
$t$	time, s
$t_c$	material balance time, s
$t_c^*$	modified material balance time, s

*Greek Symbols*

$\Delta p$	pressure difference, $\Delta p = p_i - p$ , Pa
$\Delta p^*$	transformed pressure difference for $\Delta p$ , defined in Equation (11)
$\Delta p_w$	drawdown pressure, $\Delta p_w = p_i - p_w$ , Pa
$\Delta p_w^*$	transformed pressure difference for $\Delta p_w$ , defined in Equation (11)
$\Delta t$	time step size, s
$\Delta \chi$	space step size, m
$\delta$	relative difference between the actual value and estimated value
$\mu$	fluid viscosity, Pa · s
$\rho$	fluid density, kg/m <sup>3</sup>
$v$	velocity, m/s
$\phi$	porosity
$\chi$	variable related to $r$ , defined in Equation (A52)
$\chi_e$	variable related to $r_e$ , defined in Equation (A52)
$\chi_w$	variable related to $r_w$ , defined in Equation (A52)

*Superscript*

–	Laplace space
---	---------------

*Subscript*

D	dimensionless variable
Dd	dimensionless decline variable
i	integral function
id	integral derivative function
MP	match point

**Appendix A. Derivation of the Governing Equation with the QGT**

Substituting Equation (2) into Equation (1) yields that

$$\frac{1}{r} \frac{\partial}{\partial r} \left( r \rho \frac{k}{\mu} \frac{\partial p}{\partial r} \right) = \frac{\partial(\rho \phi)}{\partial t}. \quad (\text{A1})$$

Equation (A1) can be rewritten as

$$\frac{1}{r} \rho \frac{k}{\mu} \frac{\partial p}{\partial r} + \frac{k}{\mu} \frac{\partial \rho}{\partial r} \frac{\partial p}{\partial r} + \rho \frac{\partial p}{\partial r} \frac{\partial(k/\mu)}{\partial r} + \rho \frac{k}{\mu} \frac{\partial^2 p}{\partial r^2} = \rho \frac{\partial \phi}{\partial t} + \phi \frac{\partial \rho}{\partial t}. \quad (\text{A2})$$

According to Equations (3) and (4), one can obtain that

$$\frac{\partial \rho}{\partial r} = \rho c_f \frac{\partial p}{\partial r}, \quad (\text{A3})$$

$$\frac{\partial \rho}{\partial t} = \rho c_f \frac{\partial p}{\partial t}, \quad (\text{A4})$$

$$\frac{\partial \phi}{\partial t} = \phi c_r \frac{\partial p}{\partial t}. \quad (\text{A5})$$

Substituting Equations (A3)–(A5) into Equation (A2), one can derive that

$$\frac{1}{r} \rho \frac{k}{\mu} \frac{\partial p}{\partial r} + \frac{k}{\mu} \rho c_f \left( \frac{\partial p}{\partial r} \right)^2 + \rho \frac{\partial p}{\partial r} \frac{\partial(k/\mu)}{\partial r} + \rho \frac{k}{\mu} \frac{\partial^2 p}{\partial r^2} = \rho \phi c_r \frac{\partial p}{\partial t} + \phi \rho c_f \frac{\partial p}{\partial t}. \quad (\text{A6})$$

With the assumptions of the physical model, the permeability  $k$  and fluid viscosity  $\mu$  are considered to be constant, so  $\partial(k/\mu)/\partial r = 0$  and Equation (A6) is simplified as

$$\frac{\partial^2 p}{\partial r^2} + \frac{1}{r} \frac{\partial p}{\partial r} + c_t \left( \frac{\partial p}{\partial r} \right)^2 = \frac{\phi \mu c_t}{k} \frac{\partial p}{\partial t}, \quad (\text{A7})$$

where  $c_t$  is the total compressibility expressed by  $c_t = c_f + c_r$ .

## Appendix B. Pressure Solution of Dimensionless Seepage Model under the CPP Condition

The seepage model of vertical wells in finite closed reservoirs based on the conventional governing equation can be expressed as [39]:

$$\frac{1}{r} \frac{\partial}{\partial r} \left( r \frac{\partial \Delta p}{\partial r} \right) = \frac{\phi \mu c_t}{k} \frac{\partial \Delta p}{\partial t}, \quad (\text{A8})$$

$$\Delta p|_{t=0} = 0, \quad (\text{A9})$$

$$\frac{\partial \Delta p}{\partial r} \Big|_{r=r_e} = 0, \quad (\text{A10})$$

$$\Delta p|_{r=r_w} = \Delta p_w, \quad (\text{A11})$$

where  $\Delta p = p_i - p$ .

Introducing the definitions of dimensionless variables for CPP cases listed in Table 1, the dimensionless seepage model of vertical wells in finite closed reservoirs under the CPP condition can be expressed as [39]:

$$\frac{1}{r_D} \frac{\partial}{\partial r_D} \left( r_D \frac{\partial p_D}{\partial r_D} \right) = \frac{\partial p_D}{\partial t_D}, \quad (\text{A12})$$

$$p_D|_{t_D=0} = 0, \quad (\text{A13})$$

$$\frac{\partial p_D}{\partial r_D} \Big|_{r_D=r_{eD}} = 0, \quad (\text{A14})$$

$$p_D|_{r_D=1} = 1. \quad (\text{A15})$$

Using the Laplace transform of Equations (A12)–(A15) with respect to  $t_D$  yields that [43,44]:

$$\frac{1}{r_D} \frac{\partial}{\partial r_D} \left( r_D \frac{\partial \bar{p}_D}{\partial r_D} \right) = s \bar{p}_D, \quad (\text{A16})$$

$$\frac{\partial \bar{p}_D}{\partial r_D} \Big|_{r_D=r_{eD}} = 0, \quad (\text{A17})$$

$$\bar{p}_D|_{r_D=1} = \frac{1}{s}. \quad (\text{A18})$$

The general solution of Equation (A16) is expressed by:

$$\bar{p}_D = A_1 I_0(\sqrt{s} r_D) + B_1 K_0(\sqrt{s} r_D). \quad (\text{A19})$$

Substituting Equation (A19) into Equation (A17) yields that:

$$A_1 I_1(\sqrt{s} r_{eD}) - B_1 K_1(\sqrt{s} r_{eD}) = 0. \quad (\text{A20})$$

With the aid of Equations (A18) and (A19), one can obtain that:

$$A_1 I_0(\sqrt{s}) + B_1 K_0(\sqrt{s}) = \frac{1}{s}. \quad (\text{A21})$$

Combining Equations (A20) and (A21), one can obtain that:

$$A_1 = \frac{K_1(r_{eD} \sqrt{s})}{s[I_0(\sqrt{s})K_1(r_{eD} \sqrt{s}) + K_0(\sqrt{s})I_1(r_{eD} \sqrt{s})]}, \quad (A22)$$

$$B_1 = \frac{I_1(r_{eD} \sqrt{s})}{s[I_0(\sqrt{s})K_1(r_{eD} \sqrt{s}) + K_0(\sqrt{s})I_1(r_{eD} \sqrt{s})]}. \quad (A23)$$

Substituting Equations (A22) and (A23) into Equation (A19), the pressure solution in Laplace space is derived as:

$$\bar{p}_D = \frac{K_1(r_{eD} \sqrt{s})I_0(\sqrt{s}r_D) + I_1(r_{eD} \sqrt{s})K_0(\sqrt{s}r_D)}{s[I_0(\sqrt{s})K_1(r_{eD} \sqrt{s}) + K_0(\sqrt{s})I_1(r_{eD} \sqrt{s})]}. \quad (A24)$$

### Appendix C. Bottomhole Pressure Solution of Dimensionless Seepage Model under the CRP Condition

The dimensionless seepage model of vertical wells in finite closed reservoirs under the CRP condition is expressed as [39]:

$$\frac{1}{r_D} \frac{\partial}{\partial r_D} \left( r_D \frac{\partial p_D}{\partial r_D} \right) = \frac{\partial p_D}{\partial t_D}, \quad (A25)$$

$$p_D|_{t_D=0} = 0, \quad (A26)$$

$$\frac{\partial p_D}{\partial r_D} \Big|_{r_D=r_{eD}} = 0, \quad (A27)$$

$$\left( r_D \frac{\partial p_D}{\partial r_D} \right) \Big|_{r_D=1} = -1, \quad (A28)$$

where the definitions of dimensionless variables for CRP cases are listed in Table 1.

Using the Laplace transform of Equations (A25)–(A28) with respect to  $t_D$ , one can obtain that:

$$\frac{1}{r_D} \frac{\partial}{\partial r_D} \left( r_D \frac{\partial \bar{p}_D}{\partial r_D} \right) = s \bar{p}_D, \quad (A29)$$

$$\frac{\partial \bar{p}_D}{\partial r_D} \Big|_{r_D=r_{eD}} = 0, \quad (A30)$$

$$\frac{\partial \bar{p}_D}{\partial r_D} \Big|_{r_D=1} = -\frac{1}{s}. \quad (A31)$$

The general solution of Equation (A29) is given as:

$$\bar{p}_D = A_2 I_0(\sqrt{s}r_D) + B_2 K_0(\sqrt{s}r_D). \quad (A32)$$

Substituting Equation (A32) into Equation (A30) results in that:

$$A_2 I_1(\sqrt{s}r_{eD}) - B_2 K_1(\sqrt{s}r_{eD}) = 0. \quad (A33)$$

Substituting Equation (A32) into Equation (A31) yields that:

$$A_2 I_1(\sqrt{s}) - B_2 K_1(\sqrt{s}) = -\frac{1}{s \sqrt{s}}. \quad (A34)$$

Combining Equations (A33) and (A34),  $A_2$  and  $B_2$  are determined as:

$$A_2 = \frac{K_1(r_{eD} \sqrt{s})}{s \sqrt{s} [K_1(\sqrt{s})I_1(r_{eD} \sqrt{s}) - I_1(\sqrt{s})K_1(r_{eD} \sqrt{s})]}, \quad (A35)$$

$$B_2 = \frac{I_1(r_{eD} \sqrt{s})}{s \sqrt{s} [K_1(\sqrt{s}) I_1(r_{eD} \sqrt{s}) - I_1(\sqrt{s}) K_1(r_{eD} \sqrt{s})]}. \quad (A36)$$

Substituting Equations (A35) and (A36) into Equation (A32), the dimensionless bottomhole pressure solution in Laplace space is obtained as:

$$\bar{p}_{wD} = \bar{p}_D|_{r_D=1} = \frac{K_1(r_{eD} \sqrt{s}) I_0(\sqrt{s}) + I_1(r_{eD} \sqrt{s}) K_0(\sqrt{s})}{s \sqrt{s} [K_1(\sqrt{s}) I_1(r_{eD} \sqrt{s}) - I_1(\sqrt{s}) K_1(r_{eD} \sqrt{s})]}. \quad (A37)$$

#### Appendix D. Procedure for BPDA of Production Data of Oil Wells

The procedure for BPDA of production data of oil wells is listed as follows:

(1) Computation of material balance time

$$t_c = \frac{1}{q} \int_0^t q(\tau) d\tau. \quad (A38)$$

(2) Computation of the normalized rate function

$$(q/\Delta p_w) = \frac{q}{\Delta p_w} = \frac{q}{p_i - p_w}. \quad (A39)$$

(3) Computation of the normalized rate integral function

$$(q/\Delta p_w)_i = \frac{1}{t_c} \int_0^{t_c} \frac{q}{\Delta p_w} d\tau = \frac{1}{t_c} \int_0^{t_c} \frac{q}{p_i - p_w} d\tau. \quad (A40)$$

(4) Computation of the normalized rate integral derivative function

$$(q/\Delta p_w)_{id} = -\frac{d(q/\Delta p_w)_i}{d \ln t_c} = -t_c \frac{d(q/\Delta p_w)_i}{dt_c}. \quad (A41)$$

(5) Three log-log plots of  $(q/\Delta p_w)$  vs.  $t_c$ ,  $(q/\Delta p_w)_i$  vs.  $t_c$ , and  $(q/\Delta p_w)_{id}$  vs.  $t_c$  are plotted, respectively, and then matched on Blasingame type curves shown in Figure 3. The matched  $r_{eD}$  and the match point are recorded.

(6) The formation permeability can be obtained by

$$k = \frac{B\mu}{2\pi h} \frac{(q/\Delta p_w)_{MP}}{(q_{Dd})_{MP}} \left( \ln r_{eD} - \frac{1}{2} \right), \quad (A42)$$

where  $(q/\Delta p_w)_{MP}$  is the real value of the match point,  $(q_{Dd})_{MP}$  is the dimensionless value of the match point in Blasingame type curves.

(7) The drainage radius can be calculated by

$$r_e = \sqrt{\frac{\frac{B}{c_t} \frac{(t_c)_{MP}}{(t_{cDd})_{MP}} \frac{(q/\Delta p_w)_{MP}}{(q_{Dd})_{MP}}}{\pi h \phi}}. \quad (A43)$$

(8) The effective wellbore radius and skin factor are given as, respectively

$$r_{wa} = \frac{r_e}{r_{eD}}, \quad (A44)$$

$$S = \ln \left( \frac{r_w}{r_{wa}} \right). \quad (A45)$$

(9) The original oil-in-place is estimated by

$$N = \frac{1}{c_t} \frac{(t_c)_{MP}}{(t_{cDd})_{MP}} \frac{(q/\Delta p_w)_{MP}}{(q_{Dd})_{MP}}. \quad (A46)$$

## Appendix E. Numerical Solution of Seepage Model on the Basis of the Governing Equation with the QGT

The seepage model of vertical wells in finite closed reservoirs on the basis of the governing equation with the QGT is given as [36]:

$$\frac{1}{r} \frac{\partial}{\partial r} \left( r \frac{\partial \Delta p}{\partial r} \right) - c_f \left( \frac{\partial \Delta p}{\partial r} \right)^2 = \frac{\phi \mu c_t}{k} \frac{\partial \Delta p}{\partial t}, \quad (\text{A47})$$

$$\Delta p|_{t=0} = 0, \quad (\text{A48})$$

$$\frac{\partial \Delta p}{\partial r} \Big|_{r=r_e} = 0, \quad (\text{A49})$$

$$q(t) = -\frac{2\pi kh}{\mu B} \left( r \frac{\partial \Delta p}{\partial r} \right) \Big|_{r=r_w}, \quad (\text{A50})$$

$$\Delta p_w(t) = \Delta p|_{r=r_w}, \quad (\text{A51})$$

where  $\Delta p = p_i - p$ ,  $\Delta p_w = p_i - p_w$ .

Introducing the variable  $\chi$  related to  $r$ :

$$\chi = \ln r. \quad (\text{A52})$$

Equations (A47)–(A51) are rewritten as:

$$\frac{\partial^2 \Delta p}{\partial \chi^2} - c_f \left( \frac{\partial \Delta p}{\partial \chi} \right)^2 = \frac{\phi \mu c_t}{k} e^{2\chi} \frac{\partial \Delta p}{\partial t}, \quad (\text{A53})$$

$$\Delta p|_{t=0} = 0, \quad (\text{A54})$$

$$\left( e^{-\chi} \frac{\partial \Delta p}{\partial \chi} \right) \Big|_{\chi=\chi_e} = 0, \quad (\text{A55})$$

$$q(t) = -\frac{2\pi kh}{\mu B} \frac{\partial \Delta p}{\partial \chi} \Big|_{\chi=\chi_w}, \quad (\text{A56})$$

$$\Delta p_w(t) = \Delta p|_{\chi=\chi_w}, \quad (\text{A57})$$

where  $\chi_e = \ln r_e$ ,  $\chi_w = \ln r_w$ .

Equations (A53)–(A57) are discretized by the fully implicit finite-difference method:

$$\frac{(\Delta p)_{i-1}^{j+1} - 2(\Delta p)_i^{j+1} + (\Delta p)_{i+1}^{j+1}}{(\Delta \chi)^2} - c_f \left[ \frac{(\Delta p)_i^{j+1} - (\Delta p)_{i-1}^{j+1}}{\Delta \chi} \right]^2 = \frac{\phi \mu c_t}{k} e^{2(i-1)\Delta \chi} \frac{(\Delta p)_i^{j+1} - (\Delta p)_i^j}{\Delta t}, \quad (\text{A58})$$

where  $i = 2, 3, \dots, M$ ;  $j = 0, 1, 2, \dots$ .

$$(\Delta p)_i^0 = 0, (i = 1, 2, \dots, M, M+1), \quad (\text{A59})$$

$$e^{-M\Delta \chi} \frac{(\Delta p)_{M+1}^{j+1} - (\Delta p)_M^{j+1}}{\Delta \chi} = 0, (j = 0, 1, 2, \dots), \quad (\text{A60})$$

$$q^{j+1} = -\frac{2\pi kh}{\mu B} \frac{(\Delta p)_2^{j+1} - (\Delta p)_1^{j+1}}{\Delta \chi}, (j = 0, 1, 2, \dots), \quad (\text{A61})$$

$$(\Delta p_w)^{j+1} = (\Delta p)_1^{j+1}, \quad (\text{A62})$$

where  $\Delta \chi = \chi_e/M = \ln r_e/M$ .

Equations (A58)–(A62) compose a system of nonlinear equations, which are solved by the Newton–Raphson method [45].

## References

1. He, Y.; Cheng, S.; Rui, Z.; Qin, J.; Fu, L.; Shi, J.; Wang, Y.; Li, D.; Patil, S.; Yu, H.; et al. An improved rate-transient analysis model of multi-fractured horizontal wells with non-uniform hydraulic fracture properties. *Energies* **2018**, *11*, 393. [\[CrossRef\]](#)
2. He, Y.; Cheng, S.; Li, S.; Huang, Y.; Qin, J.; Hu, L.; Yu, H. A semianalytical methodology to diagnose the locations of underperforming hydraulic fractures through pressure-transient analysis in tight gas reservoir. *SPE J.* **2017**, *22*, 924–939. [\[CrossRef\]](#)
3. Ali, A.J.; Siddiqui, S.; Dehghanpour, H. Analyzing the production data of fractured horizontal wells by a linear triple porosity model: Development of analysis equations. *J. Pet. Sci. Eng.* **2013**, *112*, 117–128. [\[CrossRef\]](#)
4. Liang, P.; Aguilera, R.; Mattar, L. *A New Method for Production Data Analysis and Well Testing Using Superposition-Rate*; Unconventional Resources Technology Conference: San Antonio, TX, USA, 2016.
5. Wang, Y.; Zhang, C.; Chen, T.; Ma, X. Modeling the nonlinear flow for a multiple-fractured horizontal well with multiple finite-conductivity fractures in triple media carbonate reservoir. *J. Porous Media* **2018**, *21*, 1283–1305. [\[CrossRef\]](#)
6. Ren, J.; Guo, P. A Novel Semi-analytical model for finite-conductivity multiple fractured horizontal wells in shale gas reservoirs. *J. Nat. Gas. Sci. Eng.* **2015**, *24*, 35–51. [\[CrossRef\]](#)
7. Ren, J.; Guo, P. Anomalous diffusion performance of multiple fractured horizontal wells in shale gas reservoirs. *J. Nat. Gas. Sci. Eng.* **2015**, *26*, 642–651. [\[CrossRef\]](#)
8. Ren, J.; Guo, P.; Peng, S.; Ma, Z. Performance of Multi-stage fractured horizontal wells with stimulated reservoir volume in tight gas reservoirs considering anomalous diffusion. *Environ. Earth Sci.* **2018**, *77*, 768. [\[CrossRef\]](#)
9. Ren, J.; Guo, P. Performance of vertical fractured wells with multiple finite-conductivity fractures. *J. Geophys. Eng.* **2015**, *12*, 978–987. [\[CrossRef\]](#)
10. Ren, J.; Guo, P.; Guo, Z.; Wang, Z. A lattice Boltzmann model for simulating gas flow in kerogen pores. *Transp. Porous Med.* **2015**, *106*, 285–301. [\[CrossRef\]](#)
11. Ren, J.; Guo, P.; Peng, S.; Yang, C. Investigation on permeability of shale matrix using the lattice Boltzmann method. *J. Nat. Gas Sci. Eng.* **2016**, *29*, 169–175. [\[CrossRef\]](#)
12. Ren, J.; Guo, P.; Guo, Z. Rectangular lattice Boltzmann equation for gaseous microscale flow. *Adv. Appl. Math. Mech.* **2016**, *8*, 306–330. [\[CrossRef\]](#)
13. Ren, J.; Guo, P. Lattice Boltzmann simulation of steady flow in a semi-elliptical cavity. *Commun. Comput. Phys.* **2017**, *21*, 692–717. [\[CrossRef\]](#)
14. Ren, J.; Zheng, Q.; Guo, P.; Peng, S.; Wang, Z.; Du, J. Pore-scale lattice Boltzmann simulation of two-component shale gas flow. *J. Nat. Gas. Sci. Eng.* **2019**, *61*, 46–70. [\[CrossRef\]](#)
15. Ren, J.; Zheng, Q.; Guo, P.; Zhao, C. Lattice Boltzmann model for gas flow through tight porous media with multiple mechanisms. *Entropy* **2019**, *21*, 133. [\[CrossRef\]](#)
16. Arps, J.J. Analysis of decline curves. *Trans. AIME* **1945**, *160*, 228–247. [\[CrossRef\]](#)
17. Ilk, D.; Rushing, J.A.; Perego, A.D.; Blasingame, T.A. *Exponential vs. Hyperbolic Decline in Tight Gas Sands: Understanding the Origin and Implications for Reserve Estimates Using Arps' Decline Curves*; SPE Annual Technical Conference and Exhibition: Denver, CO, USA, 2008.
18. Mattar, L.; Moghadam, S. *Modified Power Law Exponential Decline for Tight Gas*; Canadian International Petroleum Conference: Calgary, AB, Canada, 2009.
19. Fetkovich, M.J. Decline curve analysis using type curves. *J. Pet. Technol.* **1980**, *32*, 1065–1077. [\[CrossRef\]](#)
20. Fetkovich, M.J.; Vienot, M.E.; Bradley, M.D.; Kiesow, U.G. Decline-curve analysis using type curves—Case histories. *SPE Form. Eval.* **1987**, *2*, 637–656. [\[CrossRef\]](#)
21. Fetkovich, M.J.; Fetkovich, E.J.; Fetkovich, M.D. Useful concepts for decline-curve forecasting, reserve estimation, and analysis. *SPE Reserv. Eng.* **1996**, *11*, 13–22. [\[CrossRef\]](#)
22. Blasingame, T.A.; McCray, T.L.; Lee, W.J. *Decline Curve Analysis for Variable Pressure Drop/Variable Flowrate Systems*; SPE Gas Technology Symposium: Houston, TX, USA, 1991.
23. Palacio, J.C.; Blasingame, T.A. *Decline-Curve Analysis Using Type Curves—Analysis of Gas Well Production Data*; SPE Joint Rocky Mountain Regional and Low Permeability Reservoirs Symposium: Denver, CO, USA, 1993.



24. Doublet, L.E.; Pande, P.K.; McCollum, T.J.; Blasingame, T.A. *Decline Curve Analysis Using Type Curves-Analysis of Oil Well Production Data Using Material Balance Time: Application to Field Cases*; Petroleum Conference and Exhibition of Mexico: Veracruz, Mexico, 1994.
25. Doublet, L.E.; Blasingame, T.A. *Evaluation of Injection Well Performance Using Decline Type Curves*; SPE Permian Basin Oil and Gas Recovery Conference: Midland, TX, USA, 1996.
26. Marhaendrajana, T.; Blasingame, T.A. *Decline Curve Analysis Using Type Curves-Evaluation of Well Performance Behavior in a Multiwell Reservoir System*; Annual Technical Conference and Exhibition: New Orleans, LA, USA, 2001.
27. Pratikno, H.; Rushing, J.A.; Blasingame, T.A. *Decline Curve Analysis Using Type Curves-Fractured Wells*; SPE Annual Technical Conference and Exhibition: Denver, CO, USA, 2003.
28. Nie, R.S.; Meng, Y.F.; Jia, Y.L.; Zhang, F.X.; Yang, X.T.; Niu, X.N. Dual porosity and dual permeability modeling of horizontal well in naturally fractured reservoir. *Transp. Porous Med.* **2012**, *92*, 213–235. [[CrossRef](#)]
29. Wang, J.; Wang, X.; Dong, W. Rate Decline curves analysis of multiple-fractured horizontal wells in heterogeneous reservoirs. *J. Hydrol.* **2017**, *553*, 527–539. [[CrossRef](#)]
30. Finjord, J. *Curling up the Slope: Effects of the Quadratic Gradient Term in the Infinite-Acting Period for Two-Dimensional Reservoir Flow*; Society of Petroleum Engineers: Richardson, TX, USA, 1986.
31. Bai, M.; Ma, Q.; Roegiers, J.C. A nonlinear dual porosity model. *Appl. Math. Model.* **1994**, *18*, 602–610. [[CrossRef](#)]
32. Yao, Y.; Wu, Y.S.; Zhang, R. The transient flow analysis of fluid in a fractal, double-porosity reservoir. *Transp. Porous Med.* **2012**, *94*, 175–187. [[CrossRef](#)]
33. Lu, C.; Nie, R.S.; Guo, J.C.; Wang, D.L. Modeling the nonlinear flow behavior for horizontal well production in an underground porous-media formation. *J. Porous Media* **2015**, *18*, 43–56. [[CrossRef](#)]
34. Ren, J.; Guo, P. Nonlinear flow model of multiple fractured horizontal wells with stimulated reservoir volume including the quadratic gradient term. *J. Hydrol.* **2017**, *554*, 155–172. [[CrossRef](#)]
35. Ren, J.; Guo, P. Nonlinear seepage model for multiple fractured horizontal wells with the effect of the quadratic gradient term. *J. Porous Media* **2018**, *21*, 223–239. [[CrossRef](#)]
36. Ren, J.; Guo, P. Analytical method for transient flow rate with the effect of the quadratic gradient term. *J. Pet. Sci. Eng.* **2018**, *162*, 774–784. [[CrossRef](#)]
37. Ahmed, T. *Reservoir Engineering Handbook*; Gulf Professional Publishing: Houston, TX, USA, 2010.
38. Ren, J.; Guo, P. A general analytical method for transient flow rate with the stress-sensitive effect. *J. Hydrol.* **2018**, *565*, 262–275. [[CrossRef](#)]
39. Van Everdingen, A.F.; Hurst, W. The application of the laplace transformation to flow problems in reservoirs. *Trans. AIME* **1949**, *186*, 305–324. [[CrossRef](#)]
40. Stehfest, H. Numerical inversion of laplace transforms. *Commun. ACM* **1970**, *13*, 47–49. [[CrossRef](#)]
41. Lu, X.; Wang, Y.; Tian, F.; Li, X.; Yang, D.; Li, T.; Lv, Y.; He, X. New insights into the carbonate karstic fault system and reservoir formation in the southern tahe area of the tarim basin. *Mar. Petrol. Geol.* **2017**, *86*, 587–605. [[CrossRef](#)]
42. Mu, L.; Wang, R.; Wu, X. Development features and affecting factors of natural depletion of sandstone reservoirs in sudan. *Petrol. Explor. Develop.* **2015**, *42*, 379–383.
43. Wang, Y.; Yi, X. Transient pressure behavior of a fractured vertical well with a finite-conductivity fracture in triple media carbonate reservoir. *J. Porous Media* **2017**, *20*, 707–722. [[CrossRef](#)]
44. Wang, Y.; Yi, X. Flow Modeling of well test analysis for a multiple-fractured horizontal well in triple media carbonate reservoir. *Int. J. Nonlinear Sci. Numer. Simul.* **2018**, *19*, 439–457. [[CrossRef](#)]
45. Mathews, J.H.; Fink, K.D. *Numerical Methods Using MATLAB*, 4th ed.; Pearson: London, UK, 2004.

